THESIS

LOSS OF BEAVER DAMS DECREASES FLOODPLAIN CONNECTIVITY IN COLORADO HEADWATER STREAMS

Submitted by

Kayla Schultz

Department of Civil and Environmental Engineering

In partial fulfillment of requirements

For the Degree of Master of Science

Colorado State University

Fort Collins, Colorado

Summer 2025

Master's Committee:

Advisor: Ryan Morrison

Sara Rathburn
Peter Nelson

ABSTRACT

LOSS OF BEAVER DAMS DECREASES FLOODPLAIN CONNECTIVITY IN COLORADO HEADWATER STREAMS

As ecosystem engineers, beavers (*Castor canadensis*) modify river corridor form through dam building on lower order, low-gradient streams. The numerous geomorphic, ecological, and hydrological impacts of beaver dams are well documented, primarily through observations of active beaver systems. When beavers are removed from a system, their unmaintained dams wash out, altering the stream's hydrologic regime. The assumption that beaver dams increase floodplain connectivity is frequently presumed but has not been directly quantified. Moreover, many contemporary river restoration techniques aim to restore natural functions historically provided by beavers without fully understanding the hydrological benefits of past beaver activity. To address this knowledge gap, I quantified the change in floodplain connectivity caused by the loss of beaver dams at three headwater tributary sites in the Kawuneeche Valley, Rocky Mountain National Park, Colorado, USA. I developed two-dimensional steady-state hydraulic models to compare metrics of floodplain connectivity under historical (beaver-active) and present (no beaver activity) scenarios. The historical scenarios featured modeled beaver dams matching conditions in the year 1990 when beavers were present in the landscape. I simulated three low-to-moderate recurrence interval flood discharges to assess floodplain connectivity metrics, including the volume of water on the floodplain, the fraction of flow moving through the floodplain, the volumetric flux into the floodplain, and mean site and floodplain residence times. I found that the loss of beaver dams decreases floodplain connectivity

across all connectivity metrics (up to a 96.5% loss in connectivity) except mean floodplain residence time, which increased in the absence of dams. Channel velocities also increased following the loss of beaver dams. Results from the sensitivity analysis show that the flow state and condition of the beaver dam, modeled here by the parameters porosity and drag coefficient, can have reach-scale impacts on floodplain connectivity. Notably, while I observed floodplain disconnection at each site, the magnitude of change varied depending on both site-specific characteristics (local topography, human impacts, etc.) and on the flood magnitude. I conclude that, in headwater streams, beaver dams play an important and quantifiable role in facilitating floodplain connectivity, and floodplain disconnection from the loss of dams has major implications for other ecological and geomorphic floodplain processes. Understanding the degree and variability to which beaver dams historically promoted floodplain connectivity is especially timely considering the increasing interest in beaver-related restoration.

ACKNOWLEDGEMENTS

This project is supported through the Intermountain West Transformation Network with funding from the National Science Foundation (Grant #2115169). I also received additional funding from the Geological Society of America to support field work. This research is in collaboration with the Kawuneeche Valley Restoration Collaborative and Rocky Mountain National Park.

I am incredibly grateful to my advisor, Dr. Ryan Morrison, for his continual support and guidance throughout the research process. I am also very thankful to Dr. Sara Rathburn for her thoughtful advice and mentorship and for bringing me into this amazing research opportunity. I also want to recognize Dr. Peter Nelson for his expertise and contributions to my education in and out of the classroom. I am fortunate to have had amazing company in the field – thank you to Connor Mertz, Peter Richardson, and everyone else who joined me in the beautiful outdoors. To my lab mates, I appreciate your guidance, friendship, and many shared laughs. Finally, I would not be where I am today without the love and encouragement I have received from my close friends and family. Thank you for everything you have done for me throughout my education and life.

TABLE OF CONTENTS

LIST OF TABLES

LIST OF FIGURES

1. INTRODUCTION

As ecosystem engineers, beavers (*Castor canadensis*) modify river corridor form through dam building and maintenance (Polvi and Wohl, 2013). Beavers build and maintain dams with wood and sediment, usually across lower order streams (5th order or smaller) (Graham et al., 2020) or in floodplains and side channels of rivers with gradients less than 6%. Past researchers have documented numerous geomorphic and ecological impacts of beaver dams including their ability to attenuate and store sediment and nutrients (Meentemeyer and Butler, 1999; Pollock et al., 2007; Levine and Meyer, 2014; Wegener et al., 2017; Puttock et al., 2017), facilitate long-term floodplain aggradation (Ruedemann and Schoonmaker, 1938; Westbrook et al., 2011; Polvi and Wohl, 2012), promote floodplain carbon storage (Wohl, 2013), increase geomorphic heterogeneity (Burchsted and Daniels, 2014; Majerova et al., 2020), foster biodiversity (Smith and Mather, 2013; Law et al., 2016; Stringer and Gaywood, 2016), and increase resiliency to large disturbances (Fairfax and Whittle, 2020; Larsen et al., 2021; Jordan and Fairfax, 2022). The primary hydraulic impact of beaver dams is the upstream impoundment of water (Naiman et al., 1988; Wohl, 2021). Beaver dams can considerably alter a stream's hydrologic regime and have been shown to create wetlands (John and Klein, 2003; Adamchak et al., 2025), increase surface water storage (Hood and Bayley, 2008; Puttock et al., 2017), elevate local groundwater levels (Westbrook et al., 2006; Hill and Duval, 2009; Majerova et al., 2015), increase overbank flooding (Westbrook et al., 2006; Hill and Duval, 2009), and attenuate peak flows (Nyssen et al., 2011; Puttock et al., 2017, 2021; Neumayer et al., 2020; Graham et al., 2022).

Beaver populations are estimated to have been between 60-400 million in North America prior to European colonization, but they suffered major declines beginning in the early 17th

century due to extensive trapping and removal driven initially by the high value of beaver pelts during the European fur trade (Naiman et al., 1988). Habitat alterations, including land use changes, deforestation, in-stream large wood removal, floodplain encroachment and alteration, and the construction of flow regulating structures, concurrently altered river systems and beaver habitat, likely contributing to the ongoing loss of beavers (Beschta and Ripple, 2009; Wohl, 2021). By 1900, the North American beaver neared extinction (Naiman et al., 1988). More recently, however, the ecological benefits of beavers have become more widely recognized, and beaver populations have somewhat rebounded following efforts to regulate trapping and reintroduce beavers. Today, there are an estimated 6-12 million beavers in North America, yet many legacy effects remain that pose ongoing challenges for recovering populations (Naiman et al., 1988; Wohl, 2021).

Once beavers are removed from a river corridor, their unmaintained dams wash out resulting in shifting hydrologic and ecological regimes. The loss of beaver dams reduces spatial heterogeneity within the river corridor and encourages concentrated, single-channel flow, frequently resulting in channel incision, floodplain disconnection, and groundwater table lowering (Green and Westbrook, 2009; Wohl, 2021). Beaver dam loss is also often related to floodplain ecosystem transitions from riparian willow to alternative grassland states (Wolf et al., 2007). This ecosystem change is associated with reductions in ecosystem services, landscape resiliency, biodiversity, and flow, sediment, and nutrient attenuation (Green and Westbrook, 2009; Beschta and Ripple, 2009; Wohl, 2021).

1.1 Motivation and Rationale

The assumption that beaver dams increase floodplain connectivity is frequently presumed but has not been well quantified in previous studies. Floodplain connectivity here is defined as

the transfer of water, organisms, and materials between the channel and floodplain areas (Czuba et al., 2019). Floodplains have long been recognized for their high levels of biodiversity and biological productivity as well as for their numerous ecosystem services provided to humans (Tockner and Stanford, 2002; Petsch et al., 2023). The formation and maintenance of floodplains are driven by flood pulses (Junk et al., 1989), thus floodplain health is dependent on floodplain connectivity. Past observational studies link beaver dams to wetland creation, increased surface water storage, and increased overbank flooding, ultimately supporting the notion that beaver dams promote some level of floodplain connectivity. However, there is a lack of quantitative data that assesses the degree and variability of floodplain connectivity driven by beaver modifications.

Moreover, beaver reintroduction and beaver mimicry (e.g., the installation of beaver dam analogs, post-assisted log structures, or similar) are increasingly popular river restoration techniques used to improve stream degradation in historically beaver-occupied systems, and floodplain reconnection is a commonly stated goal of beaver-related restoration (Pollock et al., 2014; Wohl et al., 2015; Jordan and Fairfax, 2022). Restoration work, however, has outpaced research, and these techniques are implemented without fully understanding the hydrological impacts of past beaver activities (Pilliod et al., 2018). A better quantitative understanding of the relationship between beaver dams and floodplain connectivity is necessary to inform and improve future river management and restoration work (Brazier et al., 2021).

1.2 Study Objective

Based on the knowledge gaps previously identified, my research objective is to quantify the change in floodplain connectivity caused by the loss of beaver dams at three headwater tributary sites in Colorado. Using two-dimensional hydraulic surface water modeling techniques

and historical reference information, I forensically recreated historical, beaver-active conditions and compared model results with present-day conditions without beaver activity. I assessed the hydraulic impact in these systems following the loss of beaver dams using several quantitative metrics of floodplain connectivity.

2. METHODS

2.1 Study Area

My research focused on three field sites in the Kawuneeche Valley, Colorado. The Kawuneeche Valley is a wide, alluvial valley located on the western side of Rocky Mountain National Park. The valley was formed by repeated Pleistocene glaciation cycles and is bounded by mountain ranges to the east and west (Andrews, 2015). To the west is the Never Summer Range, which is composed of upper Oligocene granitic magmas underlying a Pleistocene-deposited lateral moraine. To the east, the Front Range consists of Precambrian metamorphic rocks (Westbrook et al., 2006). Wetland vegetation, including tall willow shrublands, beaver pond marshes, and fens, historically dominated valley bottom vegetation, but non-native grassland communities have become increasingly prevalent in recent decades (Cooper et al., 2025).

The valley supports the headwaters of the Upper Colorado River and several of its tributaries. The Upper Colorado River watershed's flow regime is snowmelt-dominated, and flows typically peak in late May or early June. Although the Kawuneeche Valley is now under federal management, it has a storied land use history that impacted the valley's hydrologic regime and left legacy effects still present today (Andrews, 2015). One major lasting impact is Grand Ditch, which began construction in 1890. The ditch cuts across the southwestern face of the Never Summer Range diverting water across the Continental Divide from the Colorado River basin to the South Platte River basin. To this day, Grand Ditch diverts around 50% of runoff in the Upper Colorado River watershed (Clayton and Westbrook, 2008).

Historical accounts from the mid-twentieth century documented an abundance of tall willows (*Salix* spp.), beavers' preferred food and building source, as well as sprawling beaver activity throughout the valley. A 1947 census estimated that, at that time, over 600 beavers were present throughout the Upper Colorado River watershed (Packard, 1947). Beginning in the 1980s, however, tall willow populations began to die back due to increased ungulate browsing pressure, decreasing peak flows, and fungal infection (Kaczynski et al., 2014; Andrews, 2015). The once prolific beaver populations completely abandoned the valley by the early 2000s. Today, the floodplain vegetation community has shifted from a wet beaver-willow complex to an alternative dry moose-elk-grassland state with over 90% reductions in tall willow coverage and open water areas since 1999 (Cooper et al., 2025).

In response to observed ecosystem change, Rocky Mountain National Park identified several headwater tributary sites for future ecological restoration as part of the Kawuneeche Valley Restoration Collaborative. Onahu Creek, Lower Baker Creek, and Upper Baker Creek are low-gradient, primarily single-threaded, meandering reaches historically occupied by beavers until the early 2000s (Figure 1). Site elevations range from 2663 to 2690 m. Drainage areas vary from 9 to 24 km^2, and stream reaches are similar in length (Table 1). The Upper and Lower Baker Creek drainage areas are effectively reduced in size by Grand Ditch, as reported in Table 1. I examined the relationship between the loss of beaver dams and changes in floodplain connectivity at these sites.

2.2 Field Data Collection

I collected bathymetric survey data at each study site in July 2024 using Emlid Reach RS2+ real-time kinematic (RTK) survey equipment. I surveyed channel cross sections at intervals adequate for capturing changes in bed morphology, with a mean spacing of five meters

and a maximum spacing of two bankfull widths. Cross sections extended between bank toes where banks were steep or between water surface extents where banks were gradual. I did not include the tops of banks in my cross-sectional surveys and instead retained the lidar-derived top-of-bank information in my final terrain surfaces as high-resolution lidar more accurately captures variations in banks between cross sections. To aid in aligning the bathymetry to existing lidar, I also surveyed approximately 40 top-of-bank elevations at each site and collected 15 geomorphic bankfull-width cross sections independent of the bathymetry, which I later used to validate the final terrain surface. During each survey campaign, I used two or three control points to close the survey loops. The average survey drift was 1.04 cm horizontally and 1.02 cm vertically.

Table 1. Site characteristics for Onahu Creek, Lower Baker Creek, and Upper Baker Creek. Drainage areas in parentheses indicate the total area without Grand Ditch impacts.

Site Characteristic	Onahu Creek	Lower Baker Creek	Upper Baker Creek
Drainage Area (km^2)	23.6	12.1 (25.7)	9.3 (22.0)
Stream Segment Length (km)	0.755	0.917	0.895
Mean Bed Slope (m/m)	0.005	0.003	0.003
D_{50} (mm)	32.0	22.6	22.6
D_{84} (mm)	64.0	45.0	45.0

I collected grain size distribution data by performing pebble counts at 10 transects per site. I randomly sampled 100 grains per transect using methodology described by Wolman (1954), where I paced lines across the channel bed and measured the first pebble I touched under the tip of my boot. I used a gravelometer to classify each grain size then returned samples to the channel bed downstream of the sampling area. From the pebble count data, I estimated the D_{50} and D_{84} for each site (Table 1).

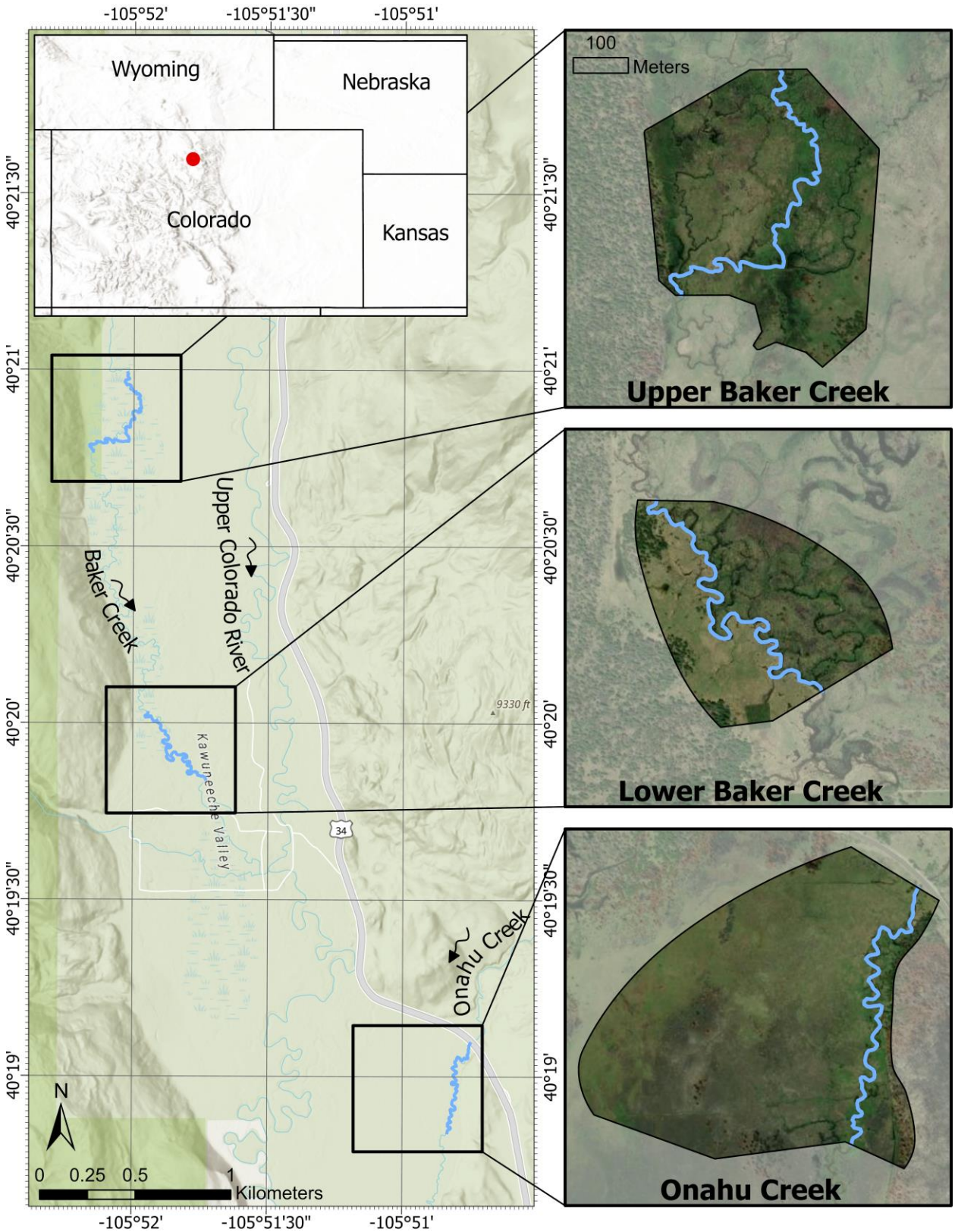

Figure 1. The three study sites are north-to-south flowing headwater tributaries located in the Kawuneeche Valley, Rocky Mountain National Park, Colorado.

For model calibration purposes, I surveyed water surface elevations (WSEL) at 10-meter intervals along each reach corresponding to a known discharge measured at the upstream site limit using a SonTek FlowTracker2 Handheld-ADV (SonTek, San Diego, California, United States). To capture conditions as close as possible to the modeled scenarios, I measured discharge on high-flow days near peak snowmelt runoff in June 2024 where flows were at or exceeding bankfull discharge. I also measured a second WSEL-discharge pair at each site, also in June 2024, for model validation purposes.

Additionally, I conducted field surveys at Onahu Creek, Lower Baker Creek, and Upper Baker Creek to document locations of remnant beaver features. These features included relict beaver berms in the floodplain and concentrations of beaver-chewed wood in the channel banks (Figure 2). I assigned each feature a confidence ranking of low, moderate, or high confidence, which I later refined in conjunction with historic aerial imagery and topographic features visible in the lidar.

Figure 2. Example of a relict floodplain feature at Onahu Creek delineated by dashed lines (photo credit: Connor Mertz).

2.3 Hydraulic Model Development

Two-dimensional (2D) hydraulic modeling offers a detailed, quantitative analysis of riverine systems, and previous studies have demonstrated its application in investigating complex channel-floodplain interactions during floods (Czuba et al., 2019; Christensen et al., 2024; Chaulagain et al., 2025). To investigate my research objectives, I generated a hybrid terrain surface using lidar and surveyed bathymetry (Section 2.3.1), developed 2D hydraulic models for each field site in the software Sedimentation and River Hydraulics Two-Dimension (SRH-2D) based on observed site conditions (Aquaveo, Provo, Utah, United States) (Section 2.3.2), calibrated and validated each model (Section 2.3.3), modified the calibrated models to recreate historical, beaver-active scenarios (Section 2.3.4), simulated several low-to-moderate steady-state flood flows for both the present and historical scenarios (Section 2.3.5), and finally compared model results at each site and for each flood discharge using several metrics of floodplain connectivity (Section 2.4).

2.3.1 Terrain Development

I developed the hydraulic model terrain surfaces from a combination of lidar and surveyed bathymetry. I obtained 2-foot (0.61-meter) hydro-flattened bare-earth Digital Elevation Models (DEMs) from August 2020 lidar acquired as part of the Colorado Water Conservation Board's multi-year effort to collect Quality Level 2 lidar for the entire state of Colorado (Colorado Water Conservation Board, 2020). Importantly, parts of the Kawuneeche Valley, including the study sites, burned at low severity during the October 2020 East Troublesome wildfire shortly after lidar collection. While it is possible there are fire-induced topographic changes not captured in the lidar, it is the most recent and spatially fine available data. Because

the hydro-flattening post-processing technique results in DEMs with smoothed water surfaces, I supplemented the lidar surface with surveyed bathymetry to improve channel geometry accuracy.

I post-processed the survey data using a CORS correction (US Department of Commerce, 2024). I then differenced the surveyed top-of-bank elevations with the lidar-derived elevations and applied an additional vertical shift for optimal lidar-bathymetry alignment. Using ArcGIS Pro, I created a 2-foot raster of just the channel bathymetry (*Create TIN* and *TIN to Raster* functions) and mosaicked each channel bathymetry raster with the lidar-derived DEMs to generate the final surfaces at each site. To validate the accuracy of the terrain surfaces, I compared bankfull areas between the raster surface and the 15 surveyed bankfull cross sections. The percent differences were 6.3%, 9.4%, and 13.7% for Onahu Creek, Lower Baker Creek, and Upper Baker Creek.

2.3.2 Model Characteristics

SRH-2D uses a finite-volume numerical method to solve the depth-averaged St. Venant equations within an unstructured mesh (Lai, 2010). Triangular mesh elements varied in dimension from 0.8 meters in the channel to 5 meters at the mesh boundary. A minimum resolution of five mesh elements spanned channel widths except at one very narrow (less than 2 meters wide) channel section at Upper Baker Creek where this was not possible. Table 2 reports the number of mesh elements and nodes within each site's model domain. I specified a constant subcritical discharge at the upstream boundary condition to simulate steady flow. Using the terrain surface and the SRH-2D Channel Calculator function, I developed a hypothetical rating curve to route water across the downstream boundary condition. One of the required inputs when generating a hypothetical rating curve is a composite Manning's *n* roughness value along the downstream boundary. At simulated flood flows, water exits the model domain through both the

channel and floodplain, so I estimated a composite Manning's *n* value considering the proportion of water exiting through the channel versus the floodplain for the particular modeled flow. Another input is channel slope, which I calculated from the terrain surface. At Onahu Creek, I added a 0.1-meter water surface elevation offset to the downstream rating curve, which was necessary to maintain model stability.

I estimated Manning's *n* values for the channel and the floodplain, then refined the channel *n* values through a calibration process. Referring to a combination of terrain data and aerial imagery, I defined the channel-floodplain boundary as the bank edge where material transitioned from mostly sediment to mostly vegetation. To calculate an initial channel Manning's *n* value, I used Limerinos' equation, which uses the D_{84} grain size and average channel hydraulic radius to compute bed roughness (Table A1) (Limerinos, 1970).

I assumed a singular Manning's *n* value to represent the floodplain and vegetated islands, which I estimated using the modified Cowan (1956) procedure as described in Arcement, Jr. and Schneider (1989) (Table A2). I did not calibrate floodplain roughness; however, my calculated floodplain Manning's *n* value (0.070 across all sites) agrees with recent studies that have quantified floodplain roughness in similarly vegetated floodplains (Prior et al., 2021; Chaulagain et al., 2022). See Appendix A for more details on Manning's *n* calculations.

2.3.3 Model Calibration and Validation

Using the highest observed discharge measured in the field and the associated surveyed WSEL, I calibrated each model by incrementally adjusting the channel Manning's *n* value to minimize the root mean squared error (RMSE) between the modeled and observed WSEL (Table A3). I validated each model using the second set of discharge-WSEL pairs. Validated Manning's *n* values are reported in Table 2.

2.3.4 Modeling Historical Beaver Dams

Referencing a September 1990 aerial image (EarthExplorer, US Geological Survey) and observations from the field, I recreated historical, beaver-active scenarios at each site. In the historical aerial imagery, I characterized potential beaver dam locations where I saw tight flow constrictions and upstream ponding. Where historical dam evidence was found both in the aerial imagery and in the field surveys, I included these as beaver dams in the modeled historical scenarios. The number of modeled dams at each site are reported in Table 2. It is worth noting that by 1990, beaver populations were no longer at historical highs, so these modeled scenarios are likely underestimates of peak beaver activity in the area.

Table 2. Selected model characteristics (MC = dams in the main channel and SC = dams in side channels).

Model Characteristic	Onahu Creek	Lower Baker Creek	Upper Baker Creek
Number of Mesh Elements	191,070	160,847	189,363
Number of Mesh Nodes	95,737	80,622	94,965
Calibrated Channel *n*	0.038	0.050	0.042
Floodplain *n* (Arcement, Jr. and Schneider, 1989)	0.070	0.070	0.070
Number of Modeled Dams	8 (MC) 2 (SC)	4 (MC) 5 (SC)	4 (MC) 5 (SC)

I modified the calibrated base models using the SRH-2D Obstructions tool to represent beaver dams. This tool allows the user to add obstructions to flow by drawing arc features and assigning them a height, width, drag coefficient, and porosity. SRH-2D then calculates and applies an additional drag force, F_d, to the affected mesh cells (Lai, 2016). The Obstructions tool was originally developed to model simply shaped, built structures like bridge piers and embankments, and I adapted it to model porous beaver dams. I drew arc features at every dam location in the approximate shape of the historical dam, and I determined the height of each dam

by either matching the height of the adjacent relict floodplain berm, if applicable, or by setting the dam height to bankfull height if no berm was observable in the lidar. I assigned each dam a width of 1.3 meters, which was the average width of relict dams visible in the lidar.

There is little consensus on the average porosity of a beaver dam, as porosity is highly dependent on the dam flow type (i.e., overflow, gapflow, throughflow, underflow, seep flow, or some combination of many flow types) (Woo and Waddington, 1990; Ronnquist and Westbrook, 2021), and flow types can change frequently over the course of a single season as beavers continually make modifications (Aguirre et al., 2024). Moreover, the measurement of beaver dam porosity is difficult and intrusive since active dams are frequently completely inundated (Nagle, 2024). One proxy for understanding beaver dam porosity is to look at human-constructed structures such as beaver dam analogs (BDAs) and post-assisted log structures (PALS). Nagle (2024) measured a series of BDAs in Washington and Idaho and found their average porosity to be 12.9%, whereas Marshall et al. (2024) looked at wood accumulation porosities and found ranges of 10 to 81% for PALS. Without active maintenance by beavers, who often pack mud and sediment onto their dams to fill pore spaces, BDAs and PALS are likely much more porous than beaver dams. Thus, I selected a somewhat conservative dam porosity estimate of 10% to represent a dam experiencing primarily overflow and some throughflow. I applied this porosity to all the modeled dams for consistency, as it is not possible to know what types of flow occurred at each dam in the 1990 scenario.

Similarly, there is limited information on the selection of a drag coefficient, C_d, for beaver dams. Several studies have investigated drag coefficients for large wood jams which function similarly to beaver dams in many cases, with results spanning a wide range of drag coefficient possibilities ($-0.05 \leq C_d \leq 9.0$) depending on the configuration of the jam and the

height of water overtopping the structure (Shields and Gippel, 1995; Gippel et al., 1996; Hygelund and Manga, 2003; Manners et al., 2007; Shields Jr. and Alonso, 2012). In the absence of better information, I selected a drag coefficient of 1.0, which is within the range suggested by Wohl et al. (2019) as part of guidance for managing for large wood and beaver dams in natural systems.

2.3.5 Model Simulations

I simulated three steady-flow discharges at Onahu Creek, Lower Baker Creek, and Upper Baker Creek for the historical and present scenarios. I obtained 2-year (Q_2), 5-year (Q_5), and 10-year (Q_{10}) peak flow values using the USGS StreamStats tool at each site, which are reported in Table 3 (StreamStats, US Geological Survey). StreamStats uses regional regression equations to estimate streamflow statistics for ungagged basins (Capesius and Stephens, 2009). One caveat to StreamStats is that regression equations in mountain regions have high standard error ranges (41-49%) and may overestimate runoff in headwater systems. Despite this high level of uncertainty, I chose to use StreamStats because the regression equations are widely available and highly accessible and are used frequently by restoration practitioners where better data are not available.

As Upper and Lower Baker Creek are impacted by Grand Ditch, I manually modified the delineated watersheds for those sites to exclude any portions of the watershed that flow into the ditch, conservatively assuming that all runoff upstream of the ditch will be conveyed out of the watershed. This process reduced the size of both watersheds by over 50%.

I chose to model low-to-moderate flood recurrence intervals because past research has suggested that beaver dams do not have major impacts on stream hydraulics for very large floods (Neumayer et al., 2020). For the 2-year, 5-year, and 10-year discharges, I ran the SRH-2D simulations until they reached steady-state conditions. Steady-state conditions are achieved when

the discharge magnitudes across the upstream and downstream model boundary conditions are equal, and the number of wetted cells is unchanging. Model outputs included water depth and velocity rasters as well as .h5 output files (format of SRH-2D files) containing node-specific data (geographic coordinates, water depth, x-velocity, and y-velocity).

Table 3. Peak flow values from USGS StreamStats tool.

Recurrence Interval	Onahu Creek	Lower Baker Creek	Upper Baker Creek
Q_2 (m^3/s)	3.77	1.90	1.72
Q_5 (m^3/s)	5.18	2.68	2.42
Q_{10} (m^3/s)	6.06	3.17	2.83

2.4 Floodplain Connectivity Metrics

I selected four primary metrics of channel-floodplain connectivity for comparison between the historical and present scenarios: volume of water on the floodplain (m^3), fraction of discharge moving through the floodplain, volumetric flux into the floodplain (m^3/s), and site mean residence time (min) (Czuba et al., 2019; Christensen et al., 2024). The volume of water on the floodplain, V_{fp}, is calculated by multiplying the inundated floodplain area, A_{fp}, by the average water depth in the floodplain, $\overline{y_{fp}}$, as shown in Equation (1). A_{fp} and $\overline{y_{fp}}$ are both calculated in ArcGIS Pro using SRH-2D model results exported as 2-foot spatial resolution raster files.

$$V_{fp} = A_{fp} * \overline{y_{fp}} \quad (1)$$

Equation (2) defines the fraction of discharge moving through the floodplain, Q_{fp}/Q_i, as the difference between the total simulated steady-state discharge, Q_i (e.g., Q_2, Q_5, etc.), and the average discharge through the primary channel, $\overline{Q_{ch}}$, divided by the total discharge, Q_i. Here,

$\overline{Q_{ch}}$ is computed using evenly spaced SRH-2D monitor lines that calculate simulated discharge every 50 meters within the channel.

$$\frac{Q_{fp}}{Q_i} = \frac{Q_i - \overline{Q_{ch}}}{Q_i} \tag{2}$$

I modified a Python script developed by Chaulagain et al. (2025) to assess volumetric channel-floodplain exchange, including the volumetric flux into the floodplain (Appendix B). Right- and left-bank control surfaces are identified as strings of individual SRH-2D mesh nodes. The flux across the face of adjacent nodes, Q_{face}, is calculated using Equation (3) as the proportion of velocity perpendicular to the face, $u_{\perp}$, multiplied by the face area, A_{face}, where positive velocities indicate flux into the floodplain and negative velocities indicate flux into the channel. Equation (4) shows that A_{face} is calculated as the distance between adjacent nodes, l_{nodes}, multiplied by the average water depth between the two nodes, $\overline{y_{nodes}}$. By summing all the positive fluxes, the total flux into the floodplain, Q_{flux}, is calculated in Equation (5).

$$Q_{face} = u_{\perp} * A_{face} \tag{3}$$

$$A_{face} = l_{nodes} * \overline{y_{nodes}} \tag{4}$$

$$Q_{flux} = \sum Q_{face} \ where \ Q_{face} > 0 \tag{5}$$

I referenced a combination of lidar, aerial imagery, and the spatial inundation extent of simulated floods to delineate right- and left-bank control surfaces in ArcGIS Pro. The control surfaces did not always overlap with the roughness-defined bank lines because in many of the scenarios there is overbanking flow that, while technically outside of the channel banks, flows in the direction of the main channel and never separates into the floodplain. For reasonable flux calculations, I

defined the flux control surfaces in a way that excludes this type of flow. See Appendix C for an illustration of flux lines relative to the roughness-defined bank lines at Lower Baker Creek.

The final floodplain connectivity metric I calculated was residence time. Equation (6) defines site mean residence time, t_{site}, as the total volume of water in the modeled site, V_{site}, divided by the total simulated steady-state discharge, Q_i.

$$t_{site} = \frac{V_{site}}{Q_i} \tag{6}$$

Equation (6) provides a reach-scale averaged residence time which is meaningful in that it represents the average time it takes for a parcel of water to move through the entire site. I also explored two approaches for calculating residence time in the floodplain only. These methods seek to isolate the mean time a water parcel spends in the floodplain. First, I followed the procedure described by Christensen et al. (2024) to calculate floodplain residence time, t_{fp}, as the volume of water in the floodplain outside of the flux control surfaces, $V_{fp,flux}$, divided by the flux into the floodplain, Q_{flux}, shown in Equation (7).

$$t_{fp} = \frac{V_{fp,flux}}{Q_{flux}} \tag{7}$$

Czuba et al. (2019) proposed another method for calculating a dimensionless floodplain residence time, $\widetilde{t_{fp}}$, normalized by channel residence time (Equation (10)). Floodplain residence time, t_{fp}, and channel residence time, t_{ch}, are calculated as the inverse of the average floodplain and channel velocities, respectively, as shown in Equation (8) and Equation (9).

$$t_{fp} = \frac{1}{\overline{u_{fp}}} \tag{8}$$

$$t_{ch} = \frac{1}{\overline{u_{ch}}} \tag{9}$$

$$\widetilde{t_{fp}} = \frac{t_{fp}}{\overline{t_{ch}}} \tag{10}$$

2.5 Sensitivity Analysis

Due to the nature of creating historical scenarios, I could not measure porosity and drag coefficient parameter values directly and instead relied on limited existing literature to estimate these values. Beaver dams vary widely in flow state and structure, so I recognize the inherent uncertainty in making parameter assumptions, and I expect that varying these parameters will have effects on model results. Therefore, I performed a sensitivity analysis at Onahu Creek to understand how varying dam porosity and drag coefficients affect modeled floodplain inundation. Using a steady discharge of 3.18 m^3/s, the peak observed discharge from stream gauge data in 2024, I varied porosity between 10%, 12.5%, and 15%, and I varied the drag coefficient between 0.5, 1.0, and 2.0. While testing a porosity value less than the modeled porosity (i.e., a porosity of 5%) would have been ideal for understanding model sensitivity, I encountered a bug in the SRH-2D Obstructions tool that limited me to a minimum porosity of 10%.

3. RESULTS

3.1 Model Calibration and Validation

Hydraulic models for each site were calibrated using WSEL surveyed at 10-meter intervals corresponding to a known discharge. I used the RMSE between the observed and modeled WSEL to assess model agreement with field conditions. I validated each calibrated *n* value using a second set of WSEL associated with a second, slightly lower-flow discharge. Those RMSE values remained low, meaning the models performed adequately under multiple flow conditions. The final calibrated channel Manning's *n* roughness values are reported in Table 4. Figure 3 shows strong agreement between the surveyed WSEL and the SRH-2D-computed WSEL for both the calibration and the validation discharges.

Although Onahu Creek has the largest median channel grain size (Table 1) and highest uncalibrated channel roughness (Table A1), the model calibration process resulted in lower in-channel Manning's *n* values at Onahu Creek compared to Lower and Upper Baker Creek. This may be attributed channel roughness characteristics not captured through grain size distributions or average channel geometry. Namely, Lower and Upper Baker Creek have somewhat irregular banks, characterized by small lobes formed by bank erosion. These features, which are not as evident on Onahu Creek, extend into the channel and contribute to increased roughness.

Table 4. Calibrated channel Manning's *n* values.

Site	Calibrated Channel Manning's *n*	Calibration Discharge (m^3/s)	Calibration RMSE (cm)	Validation Discharge (m^3/s)	Validation RMSE (cm)
Onahu Creek	0.038	2.29	4.5	1.96	8.8
Lower Baker Creek	0.050	2.40	6.1	0.93	5.2
Upper Baker Creek	0.042	2.01	5.1	1.07	5.1

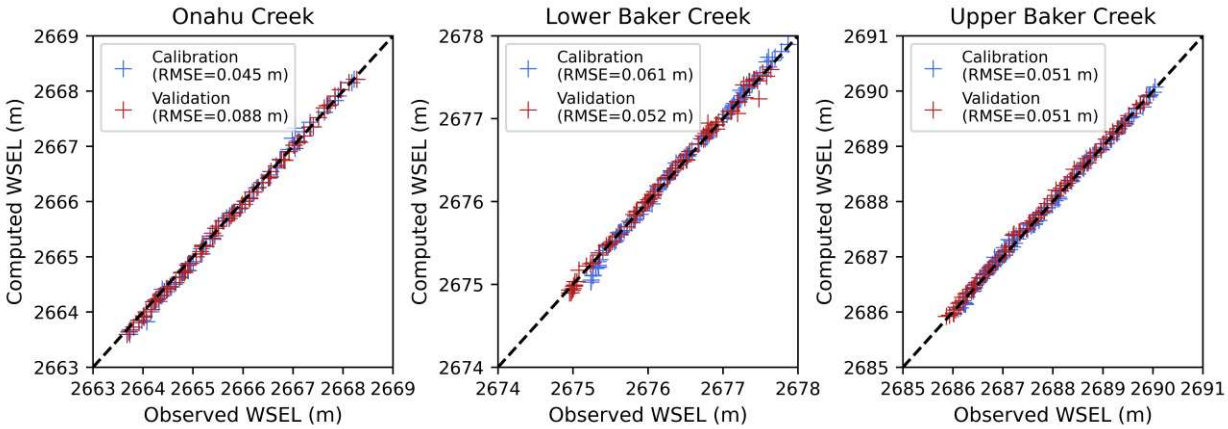

Figure 3. Evaluation of model agreement with field-observed water surface elevations (WSEL).

3.2 Model Simulations

Model results revealed systematic decreases in floodplain connection following the loss of beaver dams across all sites. Figure 4, Figure 5, and Figure 6 compare steady-state water depths between the historical (beaver-active) and present (no beaver activity) scenarios at Onahu Creek, Lower Baker Creek, and Upper Baker Creek for the 2-year, 5-year, and 10-year floods. Figure 7 shows a similar comparison of steady-state velocity for the 2-year event, and velocity plots for the 5-year and 10-year floods can be found in Appendix D (Figure D1 and Figure D2, respectively).

While each site experienced decreased floodplain activation, response characteristics varied as summarized in Table 5. At Onahu Creek, the right floodplain was highly activated while beaver dams were present (Figure 4, Figure 5, and Figure 6). Depth plots highlight relict floodplain beaver features captured in the lidar that contribute to increased routing and ponding of water. When beaver dams are not present, the channel is reduced to single-threaded flow with very little floodplain activation. At the 2-year flood (Figure 4), for example, the inundated floodplain area decreases dramatically by a factor of twelve from 45,879 m^2 to 3,816 m^2 with the

loss of beaver dams. Notably, average floodplain depth increases for all floods from the historic to present scenarios at Onahu Creek (0.103 m to 0.191 m for the 2-year flood); however, the standard deviation, σ, also increases indicating greater depth variability about the mean (Table 5).

Lower Baker Creek displays a different response to the loss of beaver dams. Here, the spatial distribution of floodplain inundation remains similar between scenarios, but the depth and area of inundated floodplain extents decreases with beaver dam loss. At the 2-year flood (Figure 4), the inundated floodplain area decreased by nearly half without beaver dams (8,142 m^2 historically compared to 4,479 m^2 at present), and mean floodplain depth was slightly lower as well (0.156 m compared to 0.154 m) (Table 5). In contrast to Onahu Creek, where beaver dams drive the shallow wetting of a large floodplain area, dams at Lower Baker Creek are less likely to activate new flow paths and instead increase the quantity of water that is diverted into side channels and relict beaver canals.

Finally, at Upper Baker Creek there is a spatial shift in floodplain activation where, historically, water wetted the right floodplain from a dam near the north edge of the site, but at present the majority of floodplain activation happens at the southeast edge of the site (Figure 4). Despite this clear spatial change in inundation extent, Upper Baker Creek experienced the smallest decrease in total inundated floodplain area following beaver dam loss (15,670 m^2 to 9,805 m^2 for the 2-year flood). Mean floodplain depth also decreased in response to the loss of beaver dams for all floods (Table 5).

Looking at the spatial distribution of velocities (Figure 7), I observed an increase in channel velocities from the historical to present scenarios at all three sites due to the decrease in roughness from the loss of in-channel obstructions. The greatest increase in channel velocity

occurred at Onahu Creek, averaging around a 50% increase for each simulated flood recurrence interval. Velocity patterns on the floodplain did not show consistent responses to dam loss, and standard deviations were high. Depending on the modeled flood discharge, mean floodplain velocity either increased or decreased at Onahu Creek and Lower Baker Creek. At Upper Baker Creek, mean floodplain velocity consistently decreased following dam loss. The high standard deviations for mean floodplain velocity suggest that a single averaged value likely does not capture the variability in floodplain velocities. Spatial changes in water depth and velocity between historical and present scenarios are visualized as raster of difference plots in Figure D3 and Figure D4, respectively.

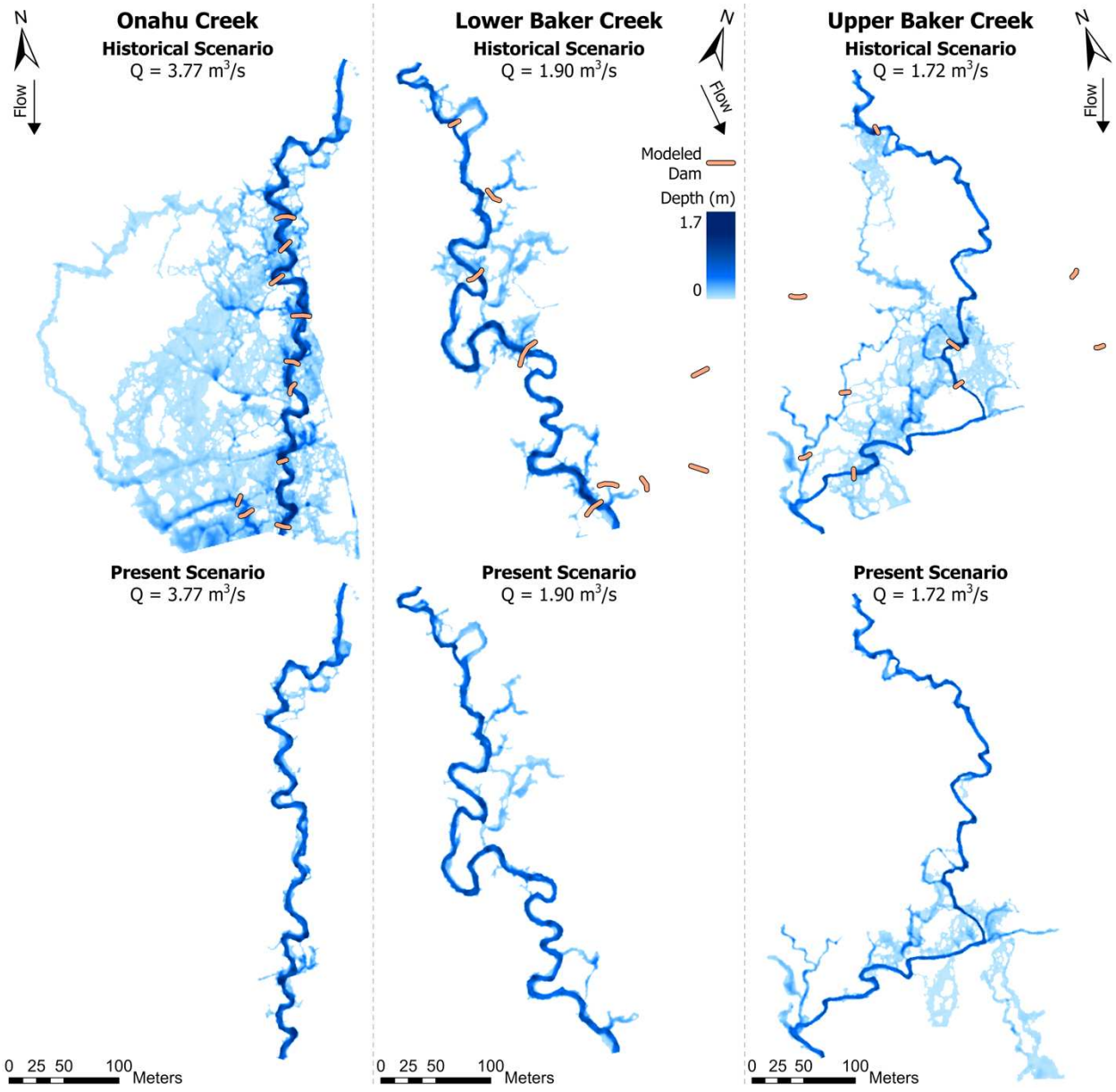

Figure 4. Steady-state depth plots for the 2-year flood.

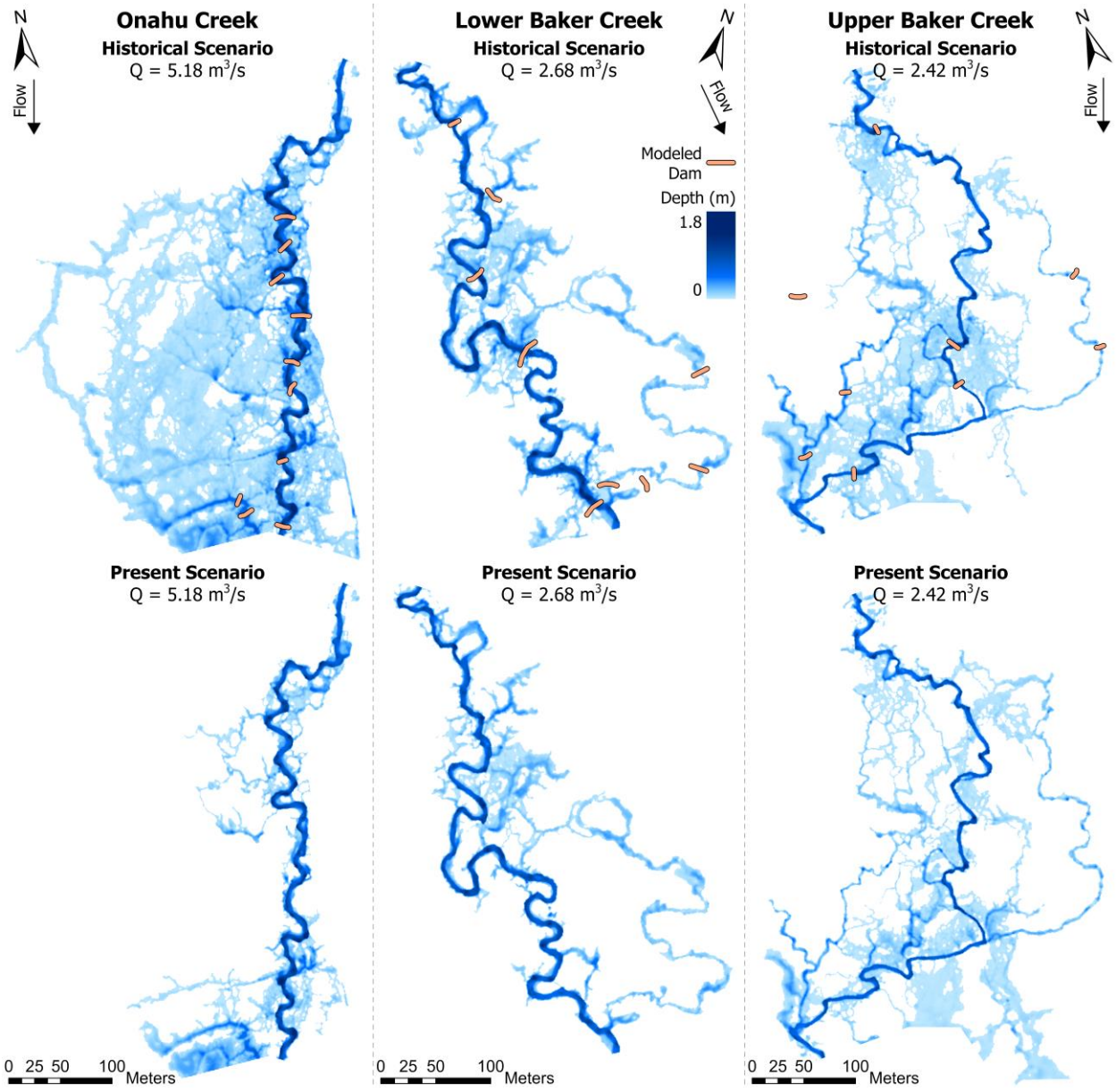

Figure 5. Steady-state depth plots for the 5-year flood.

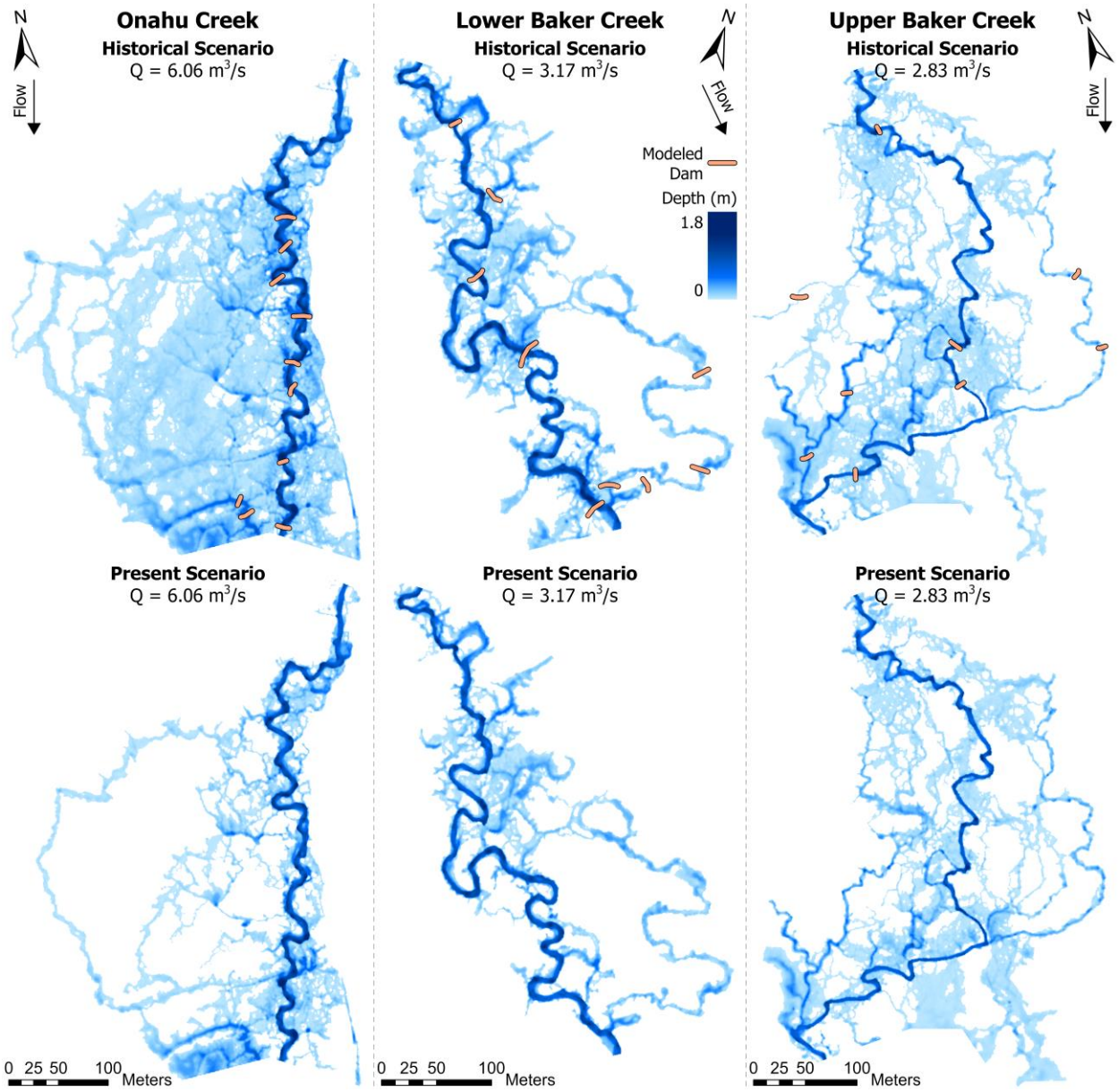

Figure 6. Steady-state depth plots for the 10-year flood.

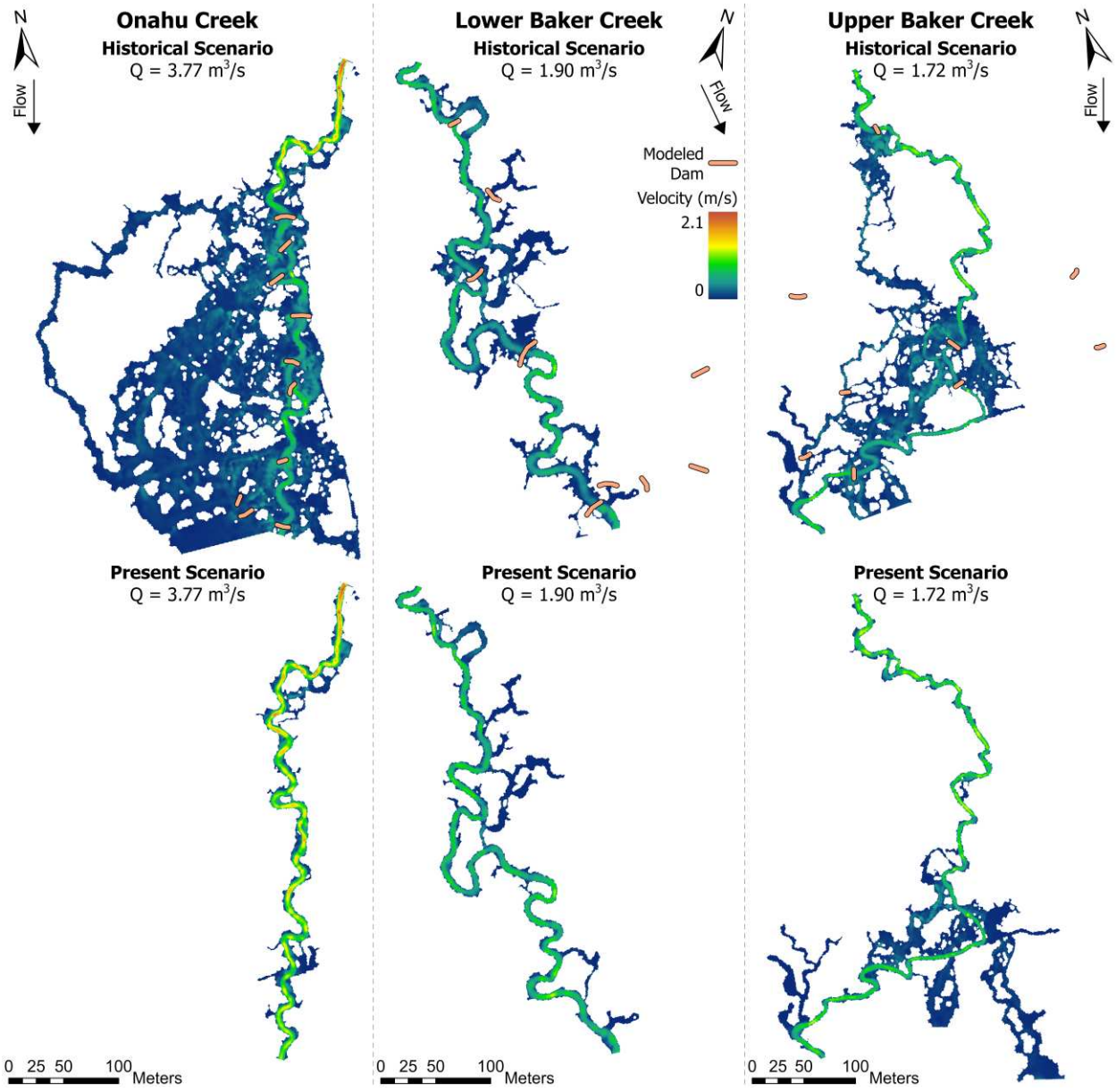

Figure 7. Steady-state velocity plots for the 2-year flood.

Table 5. Changes in inundated floodplain area (A_{fp}), mean floodplain depth ($\overline{y_{fp}}$), mean floodplain velocity ($\overline{u_{fp}}$), mean in-channel depth ($\overline{y_{ch}}$), and mean in-channel velocity ($\overline{u_{ch}}$) between historical and present scenarios and their respective standard deviations (σ).

	Historical (Beaver-Active) Scenario									**Present (No Beaver Activity) Scenario**								
	A_{fp} (m²)	$\overline{y_{fp}}$ (m)	σ y_{fp}	$\overline{u_{fp}}$ (m/s)	σ u_{fp}	$\overline{y_{ch}}$ (m)	σ y_{ch}	$\overline{u_{ch}}$ (m/s)	σ u_{ch}	A_{fp} (m²)	$\overline{y_{fp}}$ (m)	σ y_{fp}	$\overline{u_{fp}}$ (m/s)	σ u_{fp}	$\overline{y_{ch}}$ (m)	σ y_{ch}	$\overline{u_{ch}}$ (m/s)	σ u_{ch}
	Onahu Creek									***Onahu Creek***								
2-yr	45,879	0.103	0.125	0.109	0.120	0.873	0.265	0.653	0.391	3,816	0.191	0.162	0.268	0.288	0.708	0.227	0.976	0.374
5-yr	63,170	0.106	0.123	0.142	0.131	0.935	0.253	0.702	0.431	16,000	0.155	0.149	0.136	0.233	0.825	0.233	1.056	0.393
10-yr	71,158	0.110	0.124	0.158	0.137	0.964	0.248	0.724	0.453	30,237	0.121	0.137	0.121	0.200	0.876	0.232	1.087	0.408
	Lower Baker Creek									***Lower Baker Creek***								
2-yr	8,142	0.156	0.130	0.102	0.131	0.709	0.228	0.483	0.172	4,479	0.154	0.120	0.117	0.153	0.627	0.213	0.567	0.195
5-yr	20,013	0.144	0.128	0.102	0.129	0.799	0.231	0.530	0.180	13,617	0.138	0.119	0.102	0.141	0.722	0.218	0.636	0.195
10-yr	26,586	0.145	0.130	0.112	0.132	0.840	0.228	0.548	0.186	18,100	0.140	0.123	0.113	0.145	0.769	0.219	0.664	0.196
	Upper Baker Creek									***Upper Baker Creek***								
2-yr	15,670	0.096	0.102	0.124	0.116	0.589	0.227	0.565	0.235	9,805	0.092	0.107	0.085	0.126	0.572	0.227	0.645	0.271
5-yr	30,928	0.090	0.102	0.121	0.122	0.651	0.224	0.622	0.254	29,375	0.079	0.094	0.093	0.112	0.649	0.227	0.711	0.271
10-yr	43,254	0.085	0.099	0.118	0.119	0.671	0.223	0.642	0.263	39,441	0.082	0.095	0.106	0.112	0.671	0.226	0.729	0.275

3.3 Floodplain Connectivity Metrics

To quantify changes in floodplain connectivity following the loss of beaver dams, I compared several connectivity metrics between scenarios and flood recurrence intervals. All connectivity metrics decreased following the loss of beaver dams except for floodplain mean residence time. Observed decreases ranged from -12.0 to -84.6% for the volume of water on the floodplain (V_{fp}), -24.5 to -57.7% for the fraction of flow in the floodplain (Q_{fp}/Q_i), -48.7 to -96.5% for the volumetric flux into the floodplain (Q_{flux}), and -7.5 to -59.3% for site mean residence time (t_{site}) depending on the site and the flood recurrence interval (Figure 8). Volumetric flux into the floodplain and volume of water in the floodplain exhibited the greatest decreases in response to the loss of beaver dams, whereas the fraction of flow in the floodplain and site mean residence time saw more moderate declines.

Comparing responses across sites, Onahu Creek consistently displayed the greatest loss in floodplain connection across all metrics and recurrence intervals whereas Upper and Lower Baker Creek had similar, more moderate responses. In particular, Onahu Creek experienced major decreases in the volume of water on the floodplain (-53.3 to -84.6%) and volumetric flux into the floodplain (-70.8 to -95.6%) (Figure 8). These results emphasize that while each site experienced floodplain disconnection following beaver dam loss, the degree of disconnection varied across sites.

As the flood recurrence interval increases from the 2-year to the 10-year flood, floodplain connectivity increases for each metric and at each site (Figure 8). However, the relative difference between the historical and present-day scenarios decreases as flood recurrence interval increases. In other words, the greatest loss in floodplain connectivity relative to the historical scenarios occurs at the lowest recurrence interval flood (i.e., the 2-year flood). For example, the

percent difference in the volume of water on the floodplain at Onahu Creek is -84.6%, -63.0%, and -53.3% for the 2-year, 5-year, and 10-year floods respectively (Figure 8a). This consistent pattern across all metrics and sites indicates that beaver dams had the greatest influence on floodplain connectivity at smaller, more frequent discharges.

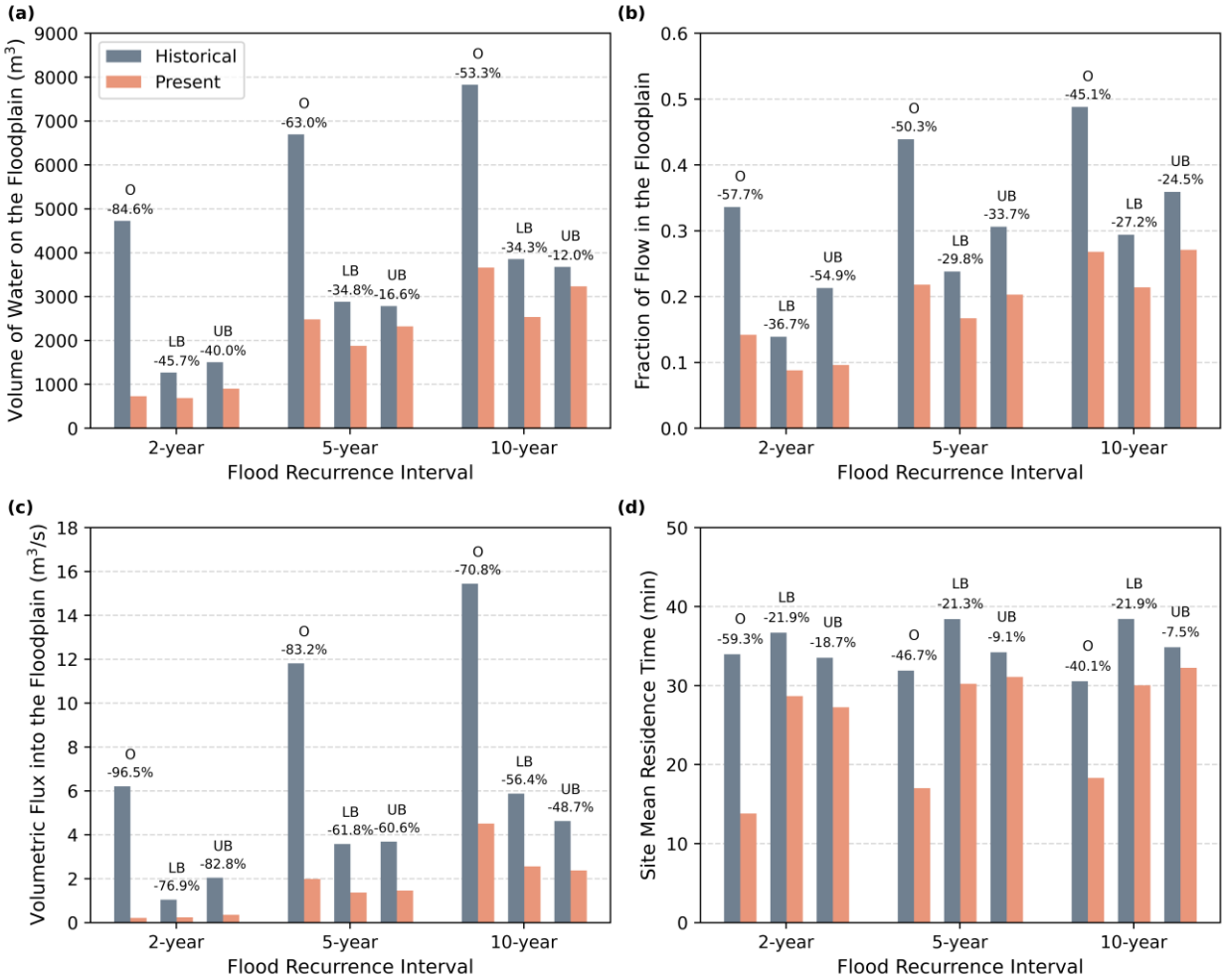

Figure 8. Metrics of floodplain connectivity at Onahu Creek (O), Lower Baker Creek (LB), and Upper Baker Creek (UB) for each modeled flood. Percentage values indicate the percent change between historical and present scenarios.

In contrast to consistent decreases in site mean residence time (Figure 8d), floodplain mean residence time generally increased in response to beaver dam loss as illustrated in Figure 9.

Floodplain mean residence time quantifies how long the average water parcel spends in the floodplain before returning to the main channel. I calculated floodplain mean residence time using two different methods: first, as the volume of water in the floodplain divided by the flux into the floodplain expressed in minutes (t_{fp}) (Christensen et al., 2024), and second, as the inverse of the average floodplain velocity normalized by the inverse of the average channel velocity expressed as a dimensionless ratio ($\widetilde{t_{fp}}$) (Czuba et al., 2019). Although it is not possible to directly compare results as the two methods do not share the same units, both methods saw similar patterns in floodplain residence time response following beaver dam loss.

Figure 9a shows that using the Christensen et al. (2024) methodology, floodplain mean residence time increased for all sites and recurrence intervals. With the exception of the 2-year flood at Onahu Creek, I noted response patterns similar to the other floodplain connectivity metrics, where the difference in floodplain residence time decreased as the flood recurrence interval increased, indicating the high influence of beaver dams at lower, more frequent flows. The greatest change in floodplain residence time was +213.4% at Upper Baker Creek at the 2-year flood, meaning that water resided in the floodplain for much longer in the absence of beaver dams.

Figure 9b illustrates increases in normalized floodplain residence time for every site and flood magnitude, again with the exception for the 2-year event at Onahu Creek. In the exception case, Onahu Creek experienced a decrease in normalized floodplain residence time at the 2-year event of -39.1%. Otherwise, response patterns using this method were somewhat variable in that there was no clear trend based on flood recurrence interval. The greatest magnitude of change at Onahu Creek happened at the 10-year flood, whereas at Lower Baker Creek it was at the 5-year flood, and at Upper Baker Creek it was at the 2-year flood.

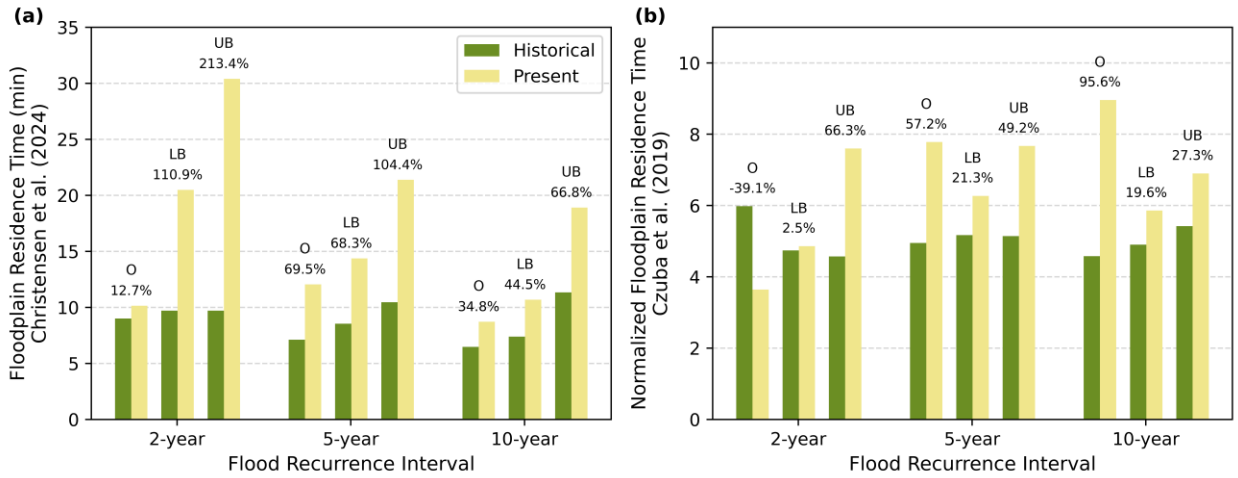

Figure 9. Comparison of mean floodplain residence time results at Onahu Creek (O), Lower Baker Creek (LB), and Upper Baker Creek (UB) for each modeled flood. Percentage values indicate the percentage change between historical and present scenarios.

3.4 Sensitivity Analysis

I modeled beaver dams using an assumed porosity and drag coefficient, though I suspected that the hydraulic models were sensitive to variations in these parameters. Thus, I conducted a sensitivity analysis to understand how varying dam porosity and drag coefficients impact model results. As the primary hydraulic impact of beaver dams is the impoundment of water (Naiman et al., 1988; Wohl, 2021), I evaluated model sensitivity by comparing changes in the volume of water on the floodplain under a single steady-state discharge at Onahu Creek. Table 6 reports differences as a percent change from the selected values. Both porosity and the drag coefficient do influence model results, with percent changes in volume of water on the floodplain as great as 30%. As porosity increases, the volume of water on the floodplain decreases. As the drag coefficient increases, the volume of water on the floodplain increases. In lieu of better historical information, assuming values for these parameters based on available literature was my only option. However, it is important to recognize that beaver dams have variable flow states which may change at relatively short temporal scales, and even minor

changes in the flow state (e.g., increasing porosity from 10.0 to 12.5%) can have reach-scale effects on channel-floodplain dynamics.

Table 6. SRH-2D obstruction sensitivity analysis results.

Porosity (%)	Drag Coefficient	Volume of Water on Floodplain (m^3)	Percent Change (%)
Varying Porosity			
10.0	1.0	3,344	N/A
12.5	1.0	2,662	-20.4
15.0	1.0	2,110	-36.9
Varying Drag Coefficient			
10.0	1.0	3,344	N/A
10.0	0.5	2,288	-31.6
10.0	2.0	4,426	32.3

4. DISCUSSION

The impacts of beaver modifications on the landscape are well documented, primarily through observations of active beaver systems (Larsen et al., 2021). Many of these observed benefits are related to the concept of floodplain connectivity; however, despite floodplain connectivity being widely recognized as beneficial (Tockner and Stanford, 2002; Petsch et al., 2023), there has been little work that quantitatively assesses the link between beaver activity and floodplain connection. My findings fill this research gap, as they support the idea that beaver-built dams play a critical role in connecting floodplains in headwater streams, thus reinforcing our foundational understanding of the hydraulic impacts of beaver dams. Results from this study also highlight how the degree of floodplain connectivity is dependent both on site-specific characteristics and on the magnitude of the flood, underscoring the nuance of historical connectivity in these systems and emphasizing the unique nature of streams, particularly in a management and restoration context.

4.1 Implications of Beaver-Induced Floodplain Connectivity

At all three headwater sites, the comparison of floodplain connectivity metrics illustrated marked decreases in connectivity following beaver dam loss. Specifically, the loss of beaver dams decreases the volume of water on the floodplain at peak flow, which elaborates on past observations that beaver dams increase surface water storage and promote wetland development (John and Klein, 2003; Puttock et al., 2017). In particular, beaver-driven wetlands increase resiliency to extreme climate events like drought by increasing water ponding and storage (Hood and Bayley, 2008) and wildfire by fostering fire-resistant riparian vegetation (Fairfax and Whittle, 2020). Increased floodplain inundation also adds complexity to riparian vegetation

succession patterns and ultimately increases landscape diversity and patchiness (Naiman et al., 1988). The reduction of floodplain ponding during floods, therefore, has negative implications for floodplain diversity and resiliency. Reduced frequency and quantity of floodplain inundation also has consequences for groundwater. Studying the main stem of the Upper Colorado River, Westbrook et al. (2006) observed that beaver dams raise groundwater elevations at both high and low flows, where the highest groundwater levels correlated to snowmelt-driven peak flow when overbank flooding occurred. Water table lowering associated with the loss of beaver dams can suppress willow growth in riparian areas as observed in Yellowstone National Park (Bilyeu et al., 2008).

Beaver dam loss also reduces the proportion of discharge moving through the floodplain relative to the main channel. When combined with increasing channel velocities, this highly channelized flow has several geomorphic implications. Maintained beaver dams promote the rapid upstream deposition of fine sediment through the reduction of in-channel velocity and stream power (Gurnell, 1998; Pollock et al., 2007; Green and Westbrook, 2009). Levine and Meyer (2014) observed changes in sediment following beaver dam breaches and concluded that most fine sediment stored upstream of dams is quickly evacuated once a dam breaks, meaning that without beaver dams, streams reduce their capacity to store and attenuate sediment. Increased channel velocities without beaver dams also may increase erosion and incision rates, as shear stresses increase and larger grain sizes can be mobilized (Green and Westbrook, 2009).

The volumetric flux into the floodplain, which more broadly represents channel-floodplain exchange, also decreases in response to the loss of beaver dams. Floodplain connectivity not only refers to the exchange of water but also the exchange of other materials including organic matter and nutrients (Czuba et al., 2019); consequently, reductions in channel-

floodplain exchange also reduces the number of possible transport pathways for nutrients and carbon to exchange and deposit on the floodplain. Wegener et al. (2017) compared wide-valley, multi-threaded reaches with beaver activity to narrow-valley, single-threaded reaches and observed high levels of floodplain nutrient and carbon storage in the beaver-occupied reaches relative to the narrow stream segments. Increased nutrient attenuation is driven by higher levels of floodplain connectivity, where nutrients are stored on the floodplain at high flows and are later available for downstream transport during receding flows. Considering organic matter specifically, wide, unconfined valley segments are disproportionately important for carbon storage. Where beaver dams are present, carbon is stored primarily in deposited floodplain sediment (Wohl et al., 2012). Moreover, the drying of floodplains associated with beaver dam loss has been shown to reduce carbon storage within the landscape (Wohl, 2013). Thus, coupled with less frequent inundation, reductions in channel-floodplain exchange following beaver dam loss not only decreases the amount of organic matter deposited in floodplains but also reduces the amount of carbon already stored.

Results from the residence time analysis paint a complicated picture, as site mean residences times decrease following beaver dam loss, but floodplain mean residence times increase. Modeled historical site mean residence times varied between 30.5 and 38.4 minutes depending on the site and flood recurrence interval. In comparison, Nagle (2024) observed water travel times through 200-meter reaches modified with beaver dam analogs to be between 22.9 and 73.5 minutes. Considering differences in reach lengths, my results show quicker water travel times. However, the flowrates between the two studies varied significantly, as I modeled flood discharges that inundated floodplains and Nagle (2024) measured water travel time during late summer when runoff was low. Majerova et al. (2015) also looked at site mean residence times

and found a similar increase associated with beaver dams, relating increasing residence times with warmer stream temperatures. Although site mean residence time decreases following beaver dam loss, floodplain mean residence time increases, suggesting that although less water is entering the floodplain, the water that does make it tends to reside for longer. This was a somewhat unintuitive result, as the presence of beaver dams also activates much greater floodplain areas, creating more opportunities for longer possible flow paths. However, using similar methodologies, Czuba et al. (2019) noted a similar inverse relationship between relative floodplain residence time and lateral exchange, where residence time increases as lateral flux decreases. Furthermore, Xiao et al. (2022) found that floodplain residence times decreased and, through Lagrangian particle tracking, particle travel distances also decreased as flood magnitudes increased from 5- to 20-year floods. Increased floodplain residence times have implications for aquatic ecosystem metabolism rates, as increased floodplain residence times from beaver dams can constrain biogeochemical processing rates as conditions transition from lentic to lotic at high flows (Wegener et al., 2017).

Floodplain flow paths are highly complex, and generalized methods employed in this study may not adequately capture the nuance of transport through the floodplain. Perhaps a more insightful way to understand residence time is through a Lagrangian particle tracking approach (Chen et al., 2020; Xiao et al., 2022). Individual particle tracking could provide a range of residence time values instead of a single average to better capture the variety of possible travel paths. This method is computationally intensive and outside of the scope of this study; however, there is an opportunity for future work to more clearly explain why floodplain residence time increases following beaver dam loss and investigate tradeoffs between floodplain connectivity and biological productivity rates.

4.2 Differences in Floodplain Connectivity Responses Across Sites

River corridors are highly complex systems, and their formation and maintenance are determined by numerous interconnected geologic, hydrologic, and biologic drivers (Castro and Thorne, 2019). Despite being geographically and geologically similar, Onahu Creek, Lower Baker Creek, and Upper Baker Creek exhibited diverse levels of floodplain connectivity with and without the influence of beaver dams, underscoring the highly influential nature of reach-scale stream characteristics. I propose at least three drivers that explain differences in floodplain connectivity responses between sites: local floodplain topography, level of beaver activity (i.e., the number of dams), and human alteration impacts. First, local topography in the adjacent floodplain varied between sites and likely influenced the preferential flow paths taken by overbanking flow. Lower Baker Creek had the highest concentration of relict side channels, including some groundwater-fed channels. These depressions were highly activated in the modeled flood scenario, and floodplain flow largely stayed within or near these site channels. In contrast, Upper Baker Creek and Onahu Creek had fewer obvious side channels, so water was more likely to travel as shallow sheet flow across a greater floodplain area.

Second, historic beaver activity at the time of the modeled scenario also appears to influence the level of observed floodplain connectivity. Onahu Creek, which showed the greatest decrease in connectivity in the absence of beaver dams, also had twice as many main-channel beaver dams as Lower and Upper Baker Creek. Higher dam density increases opportunities for water to be pushed into the floodplain.

Third, all three sites are impacted by different human alterations. At Upper and Lower Baker Creek, Grand Ditch reduces peak streamflow, thereby increasing the required recurrence interval flood necessary for overbanking flows to occur compared to historical, pre-ditch

conditions. Most likely, pre-ditch, beaver-active conditions were much wetter than what was modeled from 1990. At Onahu Creek, several abandoned historical irrigation canals still divert water west and south from the main channel at high flows. These canals contribute to floodplain topographic complexity functioning similar to beaver canals and most likely facilitate increased floodplain connectivity today.

4.3 Influences of Flood Magnitude

I observed a consistent trend across all three sites where the greatest magnitude of change in floodplain connectivity metrics occurred at smallest recurrence interval flood tested (the 2-year flood), and as flood recurrence interval increased, the difference between historic and present conditions decreased. This suggests that the loss of beaver dams has the greatest impact on floodplain connectivity at more frequent, smaller return period flows. Beavers desire ponded water behind their dams for shelter and safety from terrestrial predators as well as to increase access to foraging (Johnston, 2017). Dams are built, then, to facilitate year-round ponding, so it is logical that the greatest change in floodplain connectivity occurs at lower flows when, in the absence of in-channel obstructions, most water would otherwise be conveyed through the main channel. At high flood flows, where the channel's capacity is exceeded regardless of in-channel obstructions, the importance of beaver dams in pushing water laterally into floodplains is lessened.

When looking at peak flow attenuation, a hydraulic concept similar to floodplain connectivity, Neumayer et al. (2020) did not observe any effects from beaver dam cascades for floods greater than the 2-year recurrence interval, ultimately concluding that beaver dams may not be appropriate as flood mitigation measures. Considering floodplain connectivity, I found beaver dams to influence connection through the 10-year flood, but the diminishing nature of the

magnitude of change suggests there may be some threshold where the presence or absence of beaver dams no longer has notable impacts. Another factor when considering beaver dam impacts at high recurrence interval floods is the increasing likelihood of dam breaches. Although there is no specific flood magnitude threshold that correlates to beaver dam breaches (Andersen and Shafroth, 2010) and beaver dam durability largely depends on its condition (Westbrook et al., 2020), very large floods have higher stream power and will exert greater forces on beaver dams, increasing the possibility of breach and decreasing their reliability to facilitate floodplain connectivity.

4.4 Limitations of Modeling Approach

There are several limitations of this study which are necessary to recognize. First, hydraulic model accuracy depends on the accuracy of the modeled terrain surface. The most recent and highest quality lidar available is from August 2020. It is possible the surface has changed since then from natural channel migration, bank erosion, or other topographical changes driven by the October 2020 East Troublesome wildfire, which burned at low severity on the valley floor. The final terrain surface was built from a combination of lidar data, which defined the floodplains, and surveyed bathymetry in the channels. This surface was used for both the present and historical scenarios, although the channels likely had higher base levels and more aggraded fine sediment when beaver dams were present, altering channel form (Pollock et al., 2007).

Moreover, I recognize that there were likely landscape changes since 1990 that are not accounted for in my historical recreation process. For example, the floodplains had more woody riparian vegetation when beavers were active in the 1990s, which likely increased floodplain roughness compared to current conditions. However, I maintained the same Manning's *n* values

between the present and historical scenarios in order to minimize variables and isolate the hydraulic impacts of the presence or absence of beaver dams.

Packard (1947) recorded the highest known estimate of beaver density in the Kawuneeche Valley at around 600 beavers in the 1940s, although prior to European colonization, beaver populations were likely even higher. Declining tall willow abundance and associated shrinking beaver populations were first observed in the early 1980s (Andrews, 2015), so by 1990, the year of the historical reference image, beaver populations were no longer at historical highs. The scenarios modeled in this study, then, underrepresent the impacts of beaver activity in the area. Limited by the availability of historical reference data, the 1990 aerial imagery was the earliest available image that still offered high enough spatial resolution to identify individual dams.

As shown through the sensitivity analysis, the flow state and condition of the beaver dam, defined by its porosity and drag coefficient, are important drivers of floodplain connectivity. In the absence of more specific dam information, I assumed constant beaver dam parameters across all sites, essentially defining them as functioning in a combined overflow and throughflow state (Woo and Waddington, 1990; Ronnquist and Westbrook, 2021), which was a necessary simplification of my models.

Finally, my approach only considered surface water flow and neglected any groundwater inputs or driving factors. I observed groundwater effects driven by the close proximity of the Upper Colorado River at Upper and Lower Baker Creek. Specifically, there appeared to be groundwater inflow at both sites which was not included in the hydraulic models for simplicity.

4.5 Implications for Stream Restoration

Beaver-related restoration is an increasingly popular form of contemporary process-based restoration and has been framed as a form of climate resiliency (Beechie et al., 2010; Jordan and Fairfax, 2022). Beaver-related restoration includes beaver reintroduction as well as the construction of beaver mimicry structures such as BDAs. Floodplain reconnection is a commonly stated goal of beaver-related restoration (Wohl et al., 2015), which is underpinned by the assumption that by bringing back beavers or installing beaver dam analogs the site will see higher levels of floodplain connectivity. My findings confirm that beaver dams or similarly-functioning in-channel structures may be appropriate tools to re-establish lost floodplain connectivity in headwater streams. One caveat, however, is that human-constructed structures are likely to be much more porous than actively maintained beaver dams (Nagle, 2024; Marshall et al., 2024), so the level of attainable floodplain reconnection may not be as great as historical highs if historical beaver density is mimicked. Beavers typically build dams in densities between 2 and 18 dams per kilometer (Butler and Malanson, 2005; Wohl and Inamdar, 2025). However, a brief review of recent literature reveals BDA density is much more varied (Table 7). For instance, restoration on Bridge Creek in Oregon, USA installed BDAs at a high density of 38.3 dams/km. Ultimately, if beaver reintroduction is not possible, building restoration structures at a slightly higher density compared to historical conditions may be necessary to achieve historical levels of floodplain connectivity. However, continuing work that investigates the extent to which beaver mimicry can re-establish historical conditions would be informative for restoration practitioners and decision makers.

Table 7. Beaver dam (BD), beaver dam analog (BDA), and post-assisted log structure (PALS) densities from recent stream restoration projects in North America.

Site and Location	Number of Structures	Reach Length (km)	Average Dam Density (dams/km)
Range of observed natural beaver dam densities (Butler and Malanson, 1995; Wohl and Inamdar, 2025)	-	-	2-18
Lower Baker Creek, CO, USA (this study)	4 (BD)	0.917	4.4
Upper Baker Creek, CO, USA (this study)	4 (BD)	0.895	4.5
Onahu Creek, CO, USA (this study)	8 (BD)	0.755	10.6
South Fork Crooked River, OR, USA (Orr et al., 2020)	5 (BDA)	2.25	2.2
Pine Creek, AB, CA (Munir and Westbrook, 2021; Westbrook and Cooper, 2024)	6 (BDA)	1.072	5.6
Campbell Creek, CO, USA (Scamardo and Wohl, 2020)	7 (BDA)	0.68	10.3
Red Canyon Creek, WY, USA (Wade et al., 2020)	5 (BDA)	0.2	25.0
Fish Creek, CO, USA (Scamardo and Wohl, 2020)	8 (BDA)	0.30	26.7
Elkhorn Creek, CO, USA (pers. comm. with Ayres Associates)	8 (PALS)	0.28	28.6
Bridge Creek, OR, USA (Pollock et al., 2012; Weber et al., 2017)	134 (BDA)	3.5	38.3
Little Beaver Creek, CO, USA (pers. comm. with Ayres Associates)	12 (PALS)	0.205	58.5

The Kawuneeche Valley experienced an ecosystem transition from riparian willow to an alternative elk grassland state in response to high browsing pressure from overpopulated ungulates (Kaczynski et al., 2014). The highly studied Yellowstone National Park experienced a similar alternative state transition following the loss of the gray wolf (Wolf et al., 2007). Here, the eradication of apex predators led to intense overbrowsing of willows by elk coincident with the loss of beavers. Channel incision and groundwater table lowering following the loss of beaver dams exacerbated declining tall willows (Wolf et al., 2007). Despite the reintroduction of wolves in the 1990s, Hobbs et al. (2024) found the alternative elk grassland state remained dominant except where there were both beaver dams and reduced browsing pressure achieved through elk-exclusion fencing. Thus, the persistence of the elk grassland state is controlled both

by groundwater availability, driven by beaver-induced floodplain connectivity, and browsing intensity. Moreover, once an alternative state is realized, the system may become resistant to shifting back to riparian willow. In the Kawuneeche Valley, beaver-related restoration can increase floodplain connectivity and raise groundwater levels but may not result in a complete transition back to the pre-disturbance state. I conclude that the floodplain disconnection observed in the Kawuneeche Valley is likely one part of a complex set of drivers that led to the observed floodplain ecological transition. Floodplain reconnection as a single solution may not produce expected results without additional measures to curb browsing pressure by ungulates.

5. CONCLUSIONS

This study quantified changes in floodplain connectivity following the loss of beaver dams in several headwater streams. Results from a series of two-dimensional hydraulic models comparing present conditions with recreated historical, beaver-active scenarios demonstrated the highly influential nature of beaver dams on floodplain connectivity through the exploration of several floodplain connectivity metrics. Beaver dams are frequently assumed to have positive impacts on floodplain connectivity, and my results support that assumption with quantitative data. I found that the loss of beaver dams reduces floodplain connectivity by as much as 96.5% in headwater streams. Increasing emphasis on improving and maintaining floodplains comes following growing recognition of the numerous ecosystem services and biological benefits that floodplains provide (Tockner and Stanford, 2002; Petsch et al., 2023). Past research has highlighted many of the ecosystem services provided by beaver-occupied stream corridors including the increase of flow, sediment, and nutrient attenuation, floodplain carbon storage, biodiversity and wetland creation, resiliency to disturbance, and water storage. Results from my research confirm the foundational assumptions that other beaver dam-related research is built upon. Namely, beaver dams increase floodplain connectivity across multiple quantitative metrics, and the loss of beaver dams can considerably reduce floodplain connection in headwater streams. Understanding the extent of floodplain disconnection, and how it may vary depending on site-specific conditions and flood magnitude, is highly valuable as beaver-related restoration becomes widespread.

6. REFERENCES

Adamchak, C., Lininger, K.B., and Hinckley, E.-L.S., 2025, Animating the critical zone: beavers as critical zone engineers: Frontiers in Water, v. 7, p. 1547094, doi:10.3389/frwa.2025.1547094.

Aguirre, I., Hood, G.A., and Westbrook, C.J., 2024, Short-term dynamics of beaver dam flow states: Science of The Total Environment, v. 919, p. 170825, doi:10.1016/j.scitotenv.2024.170825.

Andersen, D.C., and Shafroth, P.B., 2010, Beaver dams, hydrological thresholds, and controlled floods as a management tool in a desert riverine ecosystem, Bill Williams River, Arizona: Ecohydrology, v. 3, p. 325–338, doi:10.1002/eco.113.

Andrews, T.G., 2015, Coyote Valley: Harvard University Press, 331 p.

Arcement, Jr., G.J., and Schneider, V.R., 1989, Guide for selecting Manning's roughness coefficients for natural channels and flood plains: United States Geological Survey Water-Supply Paper 2339, doi:10.3133/wsp2339.

Beechie, T.J., Sear, D.A., Olden, J.D., Pess, G.R., Buffington, J.M., Moir, H., Roni, P., and Pollock, M.M., 2010, Process-based Principles for Restoring River Ecosystems: BioScience, v. 60, p. 209–222, doi:10.1525/bio.2010.60.3.7.

Beschta, R.L., and Ripple, W.J., 2009, Large predators and trophic cascades in terrestrial ecosystems of the western United States: Biological Conservation, v. 142, p. 2401–2414, doi:10.1016/j.biocon.2009.06.015.

Bilyeu, D.M., Cooper, D.J., and Hobbs, N.T., 2008, Water Tables Constrain Height Recovery of Willow on Yellowstone's Northern Range: Ecological Applications, v. 18, p. 80–92, doi:10.1890/07-0212.1.

Brazier, R.E., Puttock, A., Graham, H.A., Auster, R.E., Davies, K.H., and Brown, C.M.L., 2021, Beaver: Nature's ecosystem engineers: WIREs Water, v. 8, p. e1494, doi:10.1002/wat2.1494.

Burchsted, D., and Daniels, M.D., 2014, Classification of the alterations of beaver dams to headwater streams in northeastern Connecticut, U.S.A.: Geomorphology, v. 205, p. 36–50, doi:10.1016/j.geomorph.2012.12.029.

Butler, D.R., and Malanson, G.P., 1995, Sedimentation rates and patterns in beaver ponds in a mountain environment: Geomorphology, v. 13, p. 255–269, doi:10.1016/0169-555X(95)00031-Y.

Butler, D.R., and Malanson, G.P., 2005, The geomorphic influences of beaver dams and failures of beaver dams: Geomorphology, v. 71, p. 48–60, doi:10.1016/j.geomorph.2004.08.016.

Capesius, J.P., and Stephens, V.C., 2009, Regional Regression Equations for Estimation of Natural Streamflow Statistics in Colorado: USGS Scientific Investigations Report Scientific Investigations Report 2009–5136.

Castro, J.M., and Thorne, C.R., 2019, The stream evolution triangle: Integrating geology, hydrology, and biology: River Research and Applications, v. 35, p. 315–326, doi:10.1002/rra.3421.

Chaulagain, S., Stone, M.C., Dombroski, D., Gillihan, T., Chen, L., and Zhang, S., 2022, An investigation into remote sensing techniques and field observations to model hydraulic

roughness from riparian vegetation: River Research and Applications, v. 38, p. 1730–1745, doi:10.1002/rra.4053.

Chaulagain, S., Stone, M.C., Morrison, R.R., and Byrne, C.F., 2025, Mass and Momentum Flux Prediction at the Channel-Floodplain Interface Associated With Riparian Vegetation: River Research and Applications, p. rra.4436, doi:10.1002/rra.4436.

Chen, X., Chen, L., Stone, M.C., and Acharya, K., 2020, Assessing connectivity between the river channel and floodplains during high flows using hydrodynamic modeling and particle tracking analysis: Journal of Hydrology, v. 583, p. 124609, doi:10.1016/j.jhydrol.2020.124609.

Christensen, N., Prior, E., Czuba, J., and Hession, C., 2024, Stream Restoration that Allows for Self-Adjustment Can Increase Channel-Floodplain Connectivity: Journal of Ecological Engineering Design, doi:10.21428/f69f093e.e8ffa1a3.

Clayton, J.A., and Westbrook, C.J., 2008, The effect of the Grand Ditch on the abundance of benthic invertebrates in the Colorado River, Rocky Mountain National Park: River Research and Applications, v. 24, p. 975–987, doi:10.1002/rra.1117.

Colorado Water Conservation Board, 2020, Colorado Hazard Mapping & Risk MAP Portal:, https://coloradohazardmapping.com/lidarDownload.

Cooper, D.J., Schweiger, E.W., Shaw, J.R., Westbrook, C.J., Kaczynski, K., Abouelezz, H., Esser, S.M., Nydick, K., De Silva, I., and Chimner, R.A., 2025, Rapid riparian ecosystem decline in Rocky Mountain National Park: Conservation Biology, p. e70053, doi:10.1111/cobi.70053.

Czuba, J.A., David, S.R., Edmonds, D.A., and Ward, A.S., 2019, Dynamics of Surface-Water Connectivity in a Low-Gradient Meandering River Floodplain: Water Resources Research, v. 55, p. 1849–1870, doi:10.1029/2018WR023527.

Fairfax, E., and Whittle, A., 2020, Smokey the Beaver: beaver-dammed riparian corridors stay green during wildfire throughout the western United States: Ecological Applications, v. 30, p. e02225, doi:10.1002/eap.2225.

Gippel, C.J., O'neill, I.C., Finlayson, B.L., and Schnatz, I., 1996, Hydraulic Guidelines for the Re-Introduction and Management of Large Woody Debris in Lowland Rivers: Regulated Rivers: Research & Management, v. 12, p. 223–236, doi:10.1002/(SICI)1099-1646(199603)12:2/3<223::AID-RRR391>3.0.CO;2-#.

Graham, H.A., Puttock, A.K., Elliott, M., Anderson, K., and Brazier, R.E., 2022, Exploring the dynamics of flow attenuation at a beaver dam sequence: Hydrological Processes, v. 36, p. e14735, doi:10.1002/hyp.14735.

Graham, H.A., Puttock, A., Macfarlane, W.W., Wheaton, J.M., Gilbert, J.T., Campbell-Palmer, R., Elliott, M., Gaywood, M.J., Anderson, K., and Brazier, R.E., 2020, Modelling Eurasian beaver foraging habitat and dam suitability, for predicting the location and number of dams throughout catchments in Great Britain: European Journal of Wildlife Research, v. 66, p. 42, doi:10.1007/s10344-020-01379-w.

Green, K.C., and Westbrook, C.J., 2009, Changes in riparian area structure, channel hydraulics, and sediment yield following loss of beaver dams: Journal of Ecosystems and Management, doi:10.22230/jem.2009v10n1a412.

Gurnell, A.M., 1998, The hydrogeomorphological e•ects of beaver dam-building activity: Progress in Physical Geography: Earth and Environment, v. 22, p. 167–189, doi:10.1177/030913339802200202.

Hill, A.R., and Duval, T.P., 2009, Beaver dams along an agricultural stream in southern Ontario, Canada: their impact on riparian zone hydrology and nitrogen chemistry: Hydrological Processes, v. 23, p. 1324–1336, doi:10.1002/hyp.7249.

Hobbs, N.T., Johnston, D.B., Marshall, K.N., Wolf, E.C., and Cooper, D.J., 2024, Does restoring apex predators to food webs restore ecosystems? Large carnivores in Yellowstone as a model system: Ecological Monographs, v. 94, p. e1598, doi:10.1002/ecm.1598.

Hood, G.A., and Bayley, S.E., 2008, Beaver (Castor canadensis) mitigate the effects of climate on the area of open water in boreal wetlands in western Canada: Biological Conservation, v. 141, p. 556–567, doi:10.1016/j.biocon.2007.12.003.

Hygelund, B., and Manga, M., 2003, Field measurements of drag coefficients for model large woody debris: Geomorphology, v. 51, p. 175–185, doi:10.1016/S0169-555X(02)00335-5.

John, S., and Klein, A., 2003, Beaver pond development and its hydrogeomorphic and sedimentary impact on the Jossa floodplain in Germany:

Johnston, C.A., 2017, Beavers: Boreal Ecosystem Engineers: Cham, Springer International Publishing, doi:10.1007/978-3-319-61533-2.

Jordan, C.E., and Fairfax, E., 2022, Beaver: The North American freshwater climate action plan: WIREs Water, v. 9, p. e1592, doi:10.1002/wat2.1592.

Junk, W.J., Bayley, P.B., and Sparks, R.E., 1989, The Flood Pulse Concept in River-Floodplain Systems: Proceedings of the International Large River Symposium, Canadian Special Publication of Fisheries and Aquatic Sciences, p. 110–127.

Kaczynski, K.M., Cooper, D.J., and Jacobi, W.R., 2014, Interactions of sapsuckers and *Cytospora* canker can facilitate decline of riparian willows: Botany, v. 92, p. 485–493, doi:10.1139/cjb-2014-0019.

Lai, Y.G., 2016, Modeling In-Stream Structures and Internal Features with SRH-2D: U.S. Department of the Interior, Bureau of Reclamation.

Lai, Y.G., 2010, Two-Dimensional Depth-Averaged Flow Modeling with an Unstructured Hybrid Mesh: Journal of Hydraulic Engineering, v. 136, p. 12–23, doi:10.1061/(ASCE)HY.1943-7900.0000134.

Larsen, A., Larsen, J.R., and Lane, S.N., 2021, Dam builders and their works: Beaver influences on the structure and function of river corridor hydrology, geomorphology, biogeochemistry and ecosystems: Earth-Science Reviews, v. 218, p. 103623, doi:10.1016/j.earscirev.2021.103623.

Law, A., McLean, F., and Willby, N.J., 2016, Habitat engineering by beaver benefits aquatic biodiversity and ecosystem processes in agricultural streams: Freshwater Biology, v. 61, p. 486–499, doi:10.1111/fwb.12721.

Levine, R., and Meyer, G.A., 2014, Beaver dams and channel sediment dynamics on Odell Creek, Centennial Valley, Montana, USA: Geomorphology, v. 205, p. 51–64, doi:10.1016/j.geomorph.2013.04.035.

Limerinos, J.T., 1970, Determination of the Manning Coefficient from Measured Bed Roughness in Natural Channels: U.S. Government Printing Office, 60 p.

Majerova, M., Neilson, B.T., and Roper, B.B., 2020, Beaver dam influences on streamflow hydraulic properties and thermal regimes: Science of The Total Environment, v. 718, p. 134853, doi:10.1016/j.scitotenv.2019.134853.

Majerova, M., Neilson, B.T., Schmadel, N.M., Wheaton, J.M., and Snow, C.J., 2015, Impacts of beaver dams on hydrologic and temperature regimes in a mountain stream: Hydrology and Earth System Sciences, v. 19, p. 3541–3556, doi:10.5194/hess-19-3541-2015.

Manners, R.B., Doyle, M.W., and Small, M.J., 2007, Structure and hydraulics of natural woody debris jams: Water Resources Research, v. 43, doi:10.1029/2006WR004910.

Marshall, A., Morrison, R.R., Jones, B., Triantafillou, S., and Wohl, E., 2024, Handheld lidar as a tool for characterizing wood-rich river corridors: River Research and Applications, p. rra.4239, doi:10.1002/rra.4239.

Meentemeyer, R.K., and Butler, D.R., 1999, Hydrogeomorphic Effects of Beaver Dams in Glacier National Park, Montana: Physical Geography, v. 20, p. 436–446, doi:10.1080/02723646.1999.10642688.

Munir, T.M., and Westbrook, C.J., 2021, Beaver dam analogue configurations influence stream and riparian water table dynamics of a degraded spring-fed creek in the Canadian Rockies: River Research and Applications, v. 37, p. 330–342, doi:10.1002/rra.3753.

Nagle, S., 2024, Dam dimensions and surface porosity affect the water storage capacity of Beaver dam analogs compared to natural Beaver dams: Eastern Washington University, 87 p., https://dc.ewu.edu/theses/939/.

Naiman, R.J., Johnston, C.A., and Kelley, J.C., 1988, Alteration of North American Streams by Beaver: BioScience, v. 38, p. 753–762, doi:10.2307/1310784.

Neumayer, M., Teschemacher, S., Schloemer, S., Zahner, V., and Rieger, W., 2020, Hydraulic Modeling of Beaver Dams and Evaluation of Their Impacts on Flood Events: Water, v. 12, p. 300, doi:10.3390/w12010300.

Nyssen, J., Pontzeele, J., and Billi, P., 2011, Effect of beaver dams on the hydrology of small mountain streams: Example from the Chevral in the Ourthe Orientale basin, Ardennes, Belgium: Journal of Hydrology, v. 402, p. 92–102, doi:10.1016/j.jhydrol.2011.03.008.

Orr, M.R., Weber, N.P., Noone, W.N., Mooney, M.G., Oakes, T.M., and Broughton, H.M., 2020, Short-Term Stream and Riparian Responses to Beaver Dam Analogs on a Low-Gradient Channel Lacking Woody Riparian Vegetation: Northwest Science, v. 93, p. 171–184, doi:10.3955/046.093.0302.

Packard, F.M., 1947, A Survey of the Beaver Population of Rocky Mountain National Park, Colorado: Journal of Mammalogy, v. 28, p. 219, doi:10.2307/1375171.

Petsch, D.K., Cionek, V. de M., Thomaz, S.M., and dos Santos, N.C.L., 2023, Ecosystem services provided by river-floodplain ecosystems: Hydrobiologia, v. 850, p. 2563–2584, doi:10.1007/s10750-022-04916-7.

Pilliod, D.S., Rohde, A.T., Charnley, S., Davee, R.R., Dunham, J.B., Gosnell, H., Grant, G.E., Hausner, M.B., Huntington, J.L., and Nash, C., 2018, Survey of Beaver-related Restoration Practices in Rangeland Streams of the Western USA: Environmental Management, v. 61, p. 58–68, doi:10.1007/s00267-017-0957-6.

Pollock, M.M., Beechie, T.J., and Jordan, C.E., 2007, Geomorphic changes upstream of beaver dams in Bridge Creek, an incised stream channel in the interior Columbia River basin, eastern Oregon: Earth Surface Processes and Landforms, v. 32, p. 1174–1185, doi:10.1002/esp.1553.

Pollock, M.M., Beechie, T.J., Wheaton, J.M., Jordan, C.E., Bouwes, N., Weber, N., and Volk, C., 2014, Using Beaver Dams to Restore Incised Stream Ecosystems: BioScience, v. 64, p. 279–290, doi:10.1093/biosci/biu036.

Pollock, M., Wheaton, J., Bouwes, N., Volk, C., Weber, N., and Jordan, C.E., 2012, Working with beaver to restore salmon habitat in the Bridge Creek intensively monitored watershed: Design rationale and hypotheses: NOAA Technical Memorandum NMFS-NWFSC-120,.

Polvi, L.E., and Wohl, E., 2013, Biotic Drivers of Stream Planform: Implications for Understanding the Past and Restoring the Future: BIOSCIENCE, v. 63, p. 439–452, doi:10.1525/bio.2013.63.6.6.

Polvi, L.E., and Wohl, E., 2012, The beaver meadow complex revisited – the role of beavers in post-glacial floodplain development: Earth Surface Processes and Landforms, v. 37, p. 332–346, doi:10.1002/esp.2261.

Prior, E.M., Aquilina, C.A., Czuba, J.A., Pingel, T.J., and Hession, W.C., 2021, Estimating Floodplain Vegetative Roughness Using Drone-Based Laser Scanning and Structure from Motion Photogrammetry: Remote Sensing, v. 13, p. 2616, doi:10.3390/rs13132616.

Puttock, A., Graham, H.A., Ashe, J., Luscombe, D.J., and Brazier, R.E., 2021, Beaver dams attenuate flow: A multi-site study: Hydrological Processes, v. 35, p. e14017, doi:10.1002/hyp.14017.

Puttock, A., Graham, H.A., Cunliffe, A.M., Elliott, M., and Brazier, R.E., 2017, Eurasian beaver activity increases water storage, attenuates flow and mitigates diffuse pollution from intensively-managed grasslands: Science of The Total Environment, v. 576, p. 430–443, doi:10.1016/j.scitotenv.2016.10.122.

Ronnquist, A.L., and Westbrook, C.J., 2021, Beaver dams: How structure, flow state, and landscape setting regulate water storage and release: Science of The Total Environment, v. 785, p. 147333, doi:10.1016/j.scitotenv.2021.147333.

Ruedemann, R., and Schoonmaker, W.J., 1938, Beaver-Dams as Geologic Agents: Science, v. 88, p. 523–525.

Scamardo, J., and Wohl, E., 2020, Sediment storage and shallow groundwater response to beaver dam analogues in the Colorado Front Range, USA: River Research and Applications, v. 36, p. 398–409, doi:10.1002/rra.3592.

Shields, F.D., and Gippel, C.J., 1995, Prediction of Effects of Woody Debris Removal on Flow Resistance: Journal of Hydraulic Engineering, v. 121, p. 341–354, doi:10.1061/(ASCE)0733-9429(1995)121:4(341).

Shields Jr., F.D., and Alonso, C.V., 2012, Assessment of flow forces on large wood in rivers: Water Resources Research, v. 48, doi:10.1029/2011WR011547.

Smith, J.M., and Mather, M.E., 2013, Beaver dams maintain fish biodiversity by increasing habitat heterogeneity throughout a low-gradient stream network: Freshwater Biology, v. 58, p. 1523–1538, doi:10.1111/fwb.12153.

Stringer, A.P., and Gaywood, M.J., 2016, The impacts of beavers Castor spp. on biodiversity and the ecological basis for their reintroduction to Scotland, UK: Mammal Review, v. 46, p. 270–283, doi:10.1111/mam.12068.

Tockner, K., and Stanford, J.A., 2002, Riverine flood plains: present state and future trends: Environmental Conservation, v. 29, p. 308–330, doi:10.1017/S037689290200022X.

US Department of Commerce, N. National Geodetic Survey - User Friendly CORS v4.0:, https://geodesy.noaa.gov/UFCORS/ (accessed September 2024).

US Geological Survey EarthExplorer:, https://earthexplorer.usgs.gov/ (accessed September 2024a).

US Geological Survey StreamStats:, https://streamstats.usgs.gov/ss/ (accessed November 2024b).

Wade, J., Lautz, L., Kelleher, C., Vidon, P., Davis, J., Beltran, J., and Pearce, C., 2020, Beaver dam analogues drive heterogeneous groundwater–surface water interactions: Hydrological Processes, v. 34, p. 5340–5353, doi:10.1002/hyp.13947.

Weber, N., Bouwes, N., Pollock, M.M., Volk, C., Wheaton, J.M., Wathen, G., Wirtz, J., and Jordan, C.E., 2017, Alteration of stream temperature by natural and artificial beaver dams: PLOS ONE, v. 12, p. e0176313, doi:10.1371/journal.pone.0176313.

Wegener, P., Covino, T., and Wohl, E., 2017, Beaver-mediated lateral hydrologic connectivity, fluvial carbon and nutrient flux, and aquatic ecosystem metabolism: Water Resources Research, v. 53, p. 4606–4623, doi:10.1002/2016WR019790.

Westbrook, C.J., and Cooper, D.J., 2024, Comparing the Sources of Sediment Retained by Beaver Dams and Beaver Dam Analogs: Water Resources Research, v. 60, p. e2024WR037717, doi:10.1029/2024WR037717.

Westbrook, C.J., Cooper, D.J., and Baker, B.W., 2011, Beaver assisted river valley formation: River Research and Applications, v. 27, p. 247–256, doi:10.1002/rra.1359.

Westbrook, C.J., Cooper, D.J., and Baker, B.W., 2006, Beaver dams and overbank floods influence groundwater–surface water interactions of a Rocky Mountain riparian area: Water Resources Research, v. 42, doi:10.1029/2005WR004560.

Westbrook, C.J., Ronnquist, A., and Bedard-Haughn, A., 2020, Hydrological functioning of a beaver dam sequence and regional dam persistence during an extreme rainstorm: Hydrological Processes, v. 34, p. 3726–3737, doi:10.1002/hyp.13828.

Wohl, E., 2013, Landscape-scale carbon storage associated with beaver dams: Geophysical Research Letters, v. 40, p. 3631–3636, doi:10.1002/grl.50710.

Wohl, E., 2021, Legacy effects of loss of beavers in the continental United States: Environmental Research Letters, v. 16, p. 025010, doi:10.1088/1748-9326/abd34e.

Wohl, E., Dwire, K., Sutfin, N., Polvi, L., and Bazan, R., 2012, Mechanisms of carbon storage in mountainous headwater rivers: Nature Communications, v. 3, p. 1263, doi:10.1038/ncomms2274.

Wohl, E., and Inamdar, S., 2025, Beaver Versus Human: The Big Differences in Small Dams: WIREs Water, v. 12, p. e70019, doi:10.1002/wat2.70019.

Wohl, E., Lane, S.N., and Wilcox, A.C., 2015, The science and practice of river restoration: Water Resources Research, v. 51, p. 5974–5997, doi:10.1002/2014WR016874.

Wohl, E., Scott, D.N., and Yochum, S.E., 2019, Managing for large wood and beaver dams in stream corridors: U.S. Department of Agriculture, Forest Service, Rocky Mountain Research Station RMRS-GTR-404, RMRS-GTR-404 p., doi:10.2737/RMRS-GTR-404.

Wolf, E.C., Cooper, D.J., and Hobbs, N.T., 2007, Hydrologic Regime and Herbivory Stabilize an Alternative State in Yellowstone National Park: Ecological Applications, v. 17, p. 1572–1587, doi:10.1890/06-2042.1.

Wolman, G., 1954, A method of sampling coarse river-bed material: Eos, Transactions American Geophysical Union, v. 35, p. 951–956, doi:10.1029/TR035i006p00951.

Woo, M., and Waddington, J.M., 1990, Effects of Beaver Dams on Subarctic Wetland Hydrology: Arctic, v. 43, p. 223–230.

Xiao, Y., Liu, J., Gualtieri, C., Fu, J., Gu, R., Wang, Z., Zhang, T., and Zhou, J., 2022, The effect of natural and engineered hydraulic conditions on river-floodplain connectivity using

hydrodynamic modeling and particle tracking analysis: Journal of Hydrology, v. 615, p. 128578, doi:10.1016/j.jhydrol.2022.128578.

7. APPENDICES

7.1 Appendix A: Manning's *n* Calibration and Validation

Table A1. In-channel Manning's *n* roughness estimate using Limerinos' equation (Limerinos, 1970).

	Onahu Creek	Lower Baker Creek	Upper Baker Creek
R (ft)	1.383	1.347	1.233
D_{84} (mm)	64	45	45
D_{84} (ft)	0.210	0.148	0.148
n_{ch}	0.035	0.032	0.032

Table A2. Floodplain Manning's n roughness estimate using the modified Cowan (1956) procedure detailed in Acrement and Schneider (1989) where $n_{fp} = m(n_b + n_1 + n_2 + n_3 + n_4)$.

	Onahu Creek	Lower Baker Creek	Upper Baker Creek	Justification
n_b	0.03	0.03	0.03	Firm soil, some sand.
n_1	0.018	0.018	0.018	Floodplain is irregular in shape with visible rises and sloughs from relict beaver activity and side channels.
n_2	0	0	0	N/A for floodplains.
n_3	0.002	0	0	Few scattered stumps, logs, and boulders at Onahu Creek. Negligible obstructions at Upper and Lower Baker Creek.
n_4	0.02	0.022	0.022	Dense grass and weeds, brushy, with few small stunted willows. Slightly sparser vegetation at Onahu Creek.
m	1	1	1	N/A for floodplains.
n_{fp}	0.070	0.070	0.070	

Table A3. In-channel Manning's *n* roughness calibration and validation log (bolded values are the selected *n* values).

Onahu Creek | Calibration | Q = 2.29 m^3/s				**Validation | Q = 1.96 m^3/s**	
Channel n	***Floodplain n***	***ME***	***RMSE***	***ME***	***RMSE***
0.035	0.070	-0.010	0.048		
0.036	0.070	-0.002	0.045		
0.037	0.070	-0.002	0.045		
0.038	**0.070**	0.001	0.045	-0.040	0.088
Lower Baker Creek | Calibration | Q = 2.40 m^3/s				**Validation | Q = 0.93 m^3/s**	
Channel n	***Floodplain n***	***ME***	***RMSE***	***ME***	***RMSE***
0.032	0.070	-0.064	0.095		
0.040	0.070	-0.036	0.076		

0.048	0.070	-0.005	0.062		
0.049	0.070	-0.002	0.062		
0.050	**0.070**	0.001	0.061	0.036	0.052
0.051	0.070	0.004	0.061		

Upper Baker Creek | Calibration | Q = 2.01 m^3/s				**Validation | Q = 1.07 m^3/s**	
Channel n	***Floodplain n***	***ME***	***RMSE***	***ME***	***RMSE***
0.032	0.070	-0.026	0.06		
0.040	0.070	-0.004	0.052		
0.041	0.070	-0.002	0.051		
0.042	**0.070**	0.001	0.051	0.043	0.051
0.043	0.070	0.002	0.052		

Figure A1. Example of floodplain vegetation at Upper Baker Creek in August 2024, where the floodplain is comprised primarily of grasses and sedges with no large obstructions.

7.2 Appendix B: Channel-Floodplain Flux Python Script

```
"""
This script calculates mass and momentum fluxes across left and right riverbank
boundaries using SRH-2D model outputs.

Required inputs:
    - SRH-2D model output file (.h5) containing velocity and depth data at mesh nodes
    - SRH-2D mesh file (.h5) containing mesh node coordinates
    - Time step to extract from model output file (0 is initial condition, so 1 = 2
hrs)
    - Node ID files (.csv) with SRH-2D mesh node IDs of left and right bank
boundaries
        - Must generate manually (using GIS software)
        - Node IDs do not need to be in order EXCEPT for the first point which must
be the most upstream point
        - Node IDs must be in the first column of the .csv file

Outputs:
    - .csv file containing mass and momentum fluxes across left and right banks
    - Quiver plot showing volumetric lateral flux vectors across banks

Created on 2025-03-11 by Kayla Schultz
Modified from original script by Smriti Chaulagain
"""

# %% Import Modules

import pandas as pd
import numpy as np
from math import sqrt
import h5py
import matplotlib.pyplot as plt

# %% Initialize Loop Variables

# Define lists of sites and scenarios to loop through
site = ['Onahu', 'Onahu', 'Onahu', 'Onahu', 'Onahu', 'Onahu',
        'LBaker', 'LBaker', 'LBaker', 'LBaker', 'LBaker', 'LBaker',
        'UBaker', 'UBaker', 'UBaker', 'UBaker', 'UBaker', 'UBaker']
scenario = ['2yr-Q3.77-Steady', '2yr-Q3.77-Steady-Dams',
            '5yr-Q5.18-Steady', '5yr-Q5.18-Steady-Dams',
            '10yr-Q6.06-Steady', '10yr-Q6.06-Steady-Dams',
            '2yr-Q1.90-Steady', '2yr-Q1.90-Steady-Dams',
            '5yr-Q2.68-Steady', '5yr-Q2.68-Steady-Dams',
            '10yr-Q3.17-Steady', '10yr-Q3.17-Steady-Dams',
            '2yr-Q1.72-Steady', '2yr-Q1.72-Steady-Dams',
```

```
            '5yr-Q2.42-Steady', '5yr-Q2.42-Steady-Dams',
            '10yr-Q2.83-Steady', '10yr-Q2.83-Steady-Dams']
time_step = [1, 5, 4, 2, 5, 5,
             3, 5, 9, 5, 5, 7,
             2, 7, 5, 11, 3, 7]

# %% Loop Through All Scenarios

for i in range(len(site)):

    # Set Up File Paths
    # Inputs
    model_file_path = f'./Model Outputs/{site[i]}/{scenario[i]}_XMDF.h5'
    mesh_file_path = f'./Model Outputs/{site[i]}/{site[i]}_meshes.h5'
    nodeID_leftbank_file_path = f'./Model
Outputs/{site[i]}/{site[i]}_LeftBank_Test2.csv' #######
    nodeID_rightbank_file_path = f'./Model
Outputs/{site[i]}/{site[i]}_RightBank_Test2.csv'#######
    ts = time_step[i]

    # Outputs
    output_file_path = f'./Results/Flux_{site[i]}_{scenario[i]}.csv'

    # %% Import SRH-2D Model Outputs into DataFrame

    # Load velocity and depth data from the SRH-2D model output file
    file_path = model_file_path
    f = h5py.File(file_path, 'r')
    list(f.keys())
    xvel = f['Datasets']['Velocity_m_p_s']['Values'][ts][:,0]
    yvel = f['Datasets']['Velocity_m_p_s']['Values'][ts][:,1]
    depth = f['Datasets']['Water_Depth_m']['Values'][ts]

    # # View .h5 file contents
    # with h5py.File(file_path, "r") as f:
    #     # List all groups and datasets
    #     def print_hdf5_structure(name, obj):
    #         print(name, "(Group)" if isinstance(obj, h5py.Group) else "(Dataset)")
    #     f.visititems(print_hdf5_structure)

    # Load mesh coordinates from the mesh file
    file_path = mesh_file_path
    j = h5py.File(file_path, 'r')
    coordinates = np.zeros((len(j['2DMeshModule'][f'{site[i]}
Mesh']['Nodes']['NodeLocs'][:,0]),2))
    coordinates[:,0] = j['2DMeshModule'][f'{site[i]} Mesh']['Nodes']['NodeLocs'][:,0]
# x coordinates
```

```
    coordinates[:,1] = j['2DMeshModule'][f'{site[i]} Mesh']['Nodes']['NodeLocs'][:,1]
# y coordinates

    # Merge into a DataFrame (x-coordinate, y-coordinate, depth, x-velocity, y-
velocity)
    srh2d = pd.DataFrame({
        'X_m': coordinates[:,0],
        'Y_m': coordinates[:,1],
        'Water_Depth_m': depth,
        'Vel_X_mps': xvel,
        'Vel_Y_mps': yvel
    })
    srh2d.replace(-999, 0, inplace=True) # replace nodata values with 0
    srh2d.head()

    # %% Read Node ID Files

    nodeID_left = pd.read_csv(nodeID_leftbank_file_path)
    nodeID_right = pd.read_csv(nodeID_rightbank_file_path)

    nodeID_left.head()
    nodeID_right.head()

    # %% Extract Right Bank Data Based on Node ID

    # Convert node IDs to 0-based index for Pandas
    node_ids = nodeID_right.iloc[:, 0] - 1
    node_ids = node_ids[node_ids.isin(srh2d.index - 1)] # Filter valid IDs

    # Create file with right bank data from srh2d based on node IDs
    rb_model_output = srh2d.loc[node_ids].copy()
    rb_model_output.insert(0, 'Node_ID', node_ids.values + 1)
    # Keep only the relevant columns (Node_ID, x, y, depth, xvel, yvel)
    rb_model_output = rb_model_output.iloc[:, 0:6]

    rb_model_output.head()

    # %% Extract Left Bank Data Based on Node ID

    # Convert node IDs to 0-based index for Pandas
    node_ids = nodeID_left.iloc[:, 0] - 1
    node_ids = node_ids[node_ids.isin(srh2d.index - 1)] # Filter valid IDs

    # Create file with left bank data from srh2d based on node IDs
    lb_model_output = srh2d.loc[node_ids].copy()
    lb_model_output.insert(0, 'Node_ID', node_ids.values + 1)
    # Keep only the relevant columns (Node_ID, x, y, depth, xvel, yvel)
```

```
    lb_model_output = lb_model_output.iloc[:, 0:6]

    lb_model_output.head()

    # %% Sort Bank Nodes Spatially From Upstream to Downstream

    # IMPOTANT: the first node in the DataFrame must be the upstream-most node
    def sort_nodes_spatially(df):
        # Extract x, y coordinates
        coords = df.iloc[:, 1:3].values

        # Initialize sorted order
        sorted_indices = [0]  # Start with the first row
        remaining_indices = set(range(1, len(df)))  # Remaining indices to be sorted

        while remaining_indices:
            last_idx = sorted_indices[-1]
            last_coord = coords[last_idx]

            # Find the nearest neighbor
            nearest_idx = min(remaining_indices, key=lambda i:
np.linalg.norm(coords[i] - last_coord))
            sorted_indices.append(nearest_idx)
            remaining_indices.remove(nearest_idx)

        # Return sorted DataFrame
        return df.iloc[sorted_indices].reset_index(drop=True)

    sorted_rb_model_output = sort_nodes_spatially(rb_model_output)
    sorted_rb_model_output.head()

    sorted_lb_model_output = sort_nodes_spatially(lb_model_output)
    sorted_lb_model_output.head()

    # %% Define Boundary Types for Assigning Unit Vector Direction

    boundary_type_r = 0 # right bank
    boundary_type_l = 1 # left bank

    # %% Define Function for Unit Vectors

    def normals(boundary_type, node_data):
        xx = []
        yy = []
        uu = []
        vv = []
```

```
        i = len(node_data.iloc[:,1])
        for n in range(0, i-1): # Iterate through each pair of consecutive nodes to
define a segment along the bank

            x = (node_data.iloc[n, 1] + node_data.iloc[n + 1, 1]) / 2  # midpoint x
            y = (node_data.iloc[n, 2] + node_data.iloc[n + 1, 2]) / 2  # midpoint y

            dx = node_data.iloc[n + 1, 1] - node_data.iloc[n, 1]  # change in x
            dy = node_data.iloc[n + 1, 2] - node_data.iloc[n, 2]  # change in y

            # Compute unit normal vector (u, v)
            mag = (dx**2 + dy**2) ** 0.5

            if mag != 0:
                u = -dy / mag  # unit normal x-component
                v = dx / mag   # unit normal y-component
            else:
                u, v = 0, 0  # In case the points are the same (should not normally
happen)

            # Ensure unit vector points into floodplain from river bank by checking
relative position of consecutive nodes
            if (boundary_type == 0): # Right bank
                if (node_data.iloc[n,1] < node_data.iloc[n+1,1]) &
(node_data.iloc[n,2] > node_data.iloc[n+1,2]): # downward to the right
                    u = abs(u) * -1
                    v = abs(v) * -1
                elif (node_data.iloc[n,1] > node_data.iloc[n+1,1]) &
(node_data.iloc[n,2] > node_data.iloc[n+1,2]): # downward to the left
                    u = abs(u) * -1
                    v = abs(v)
                elif (node_data.iloc[n,1] < node_data.iloc[n+1,1]) &
(node_data.iloc[n,2] < node_data.iloc[n+1,2]): # upward to the right
                    u = abs(u)
                    v = abs(v) * -1
                elif (node_data.iloc[n,1] > node_data.iloc[n+1,1]) &
(node_data.iloc[n,2] < node_data.iloc[n+1,2]): # upward to the left
                    u = abs(u)
                    v = abs(v)
                elif (node_data.iloc[n,1] == node_data.iloc[n+1,1]) &
(node_data.iloc[n,2] > node_data.iloc[n+1,2]): # vertical downward
                    u = -1
                    v = 0
                elif (node_data.iloc[n,1] == node_data.iloc[n+1,1]) &
(node_data.iloc[n,2] < node_data.iloc[n+1,2]): # vertical upward
                    u = 1
                    v = 0
```

```
                elif (node_data.iloc[n,1] > node_data.iloc[n+1,1]) &
(node_data.iloc[n,2] == node_data.iloc[n+1,2]): # horizontal leftward
                    u = 0
                    v = 1
                elif (node_data.iloc[n,1] < node_data.iloc[n+1,1]) &
(node_data.iloc[n,2] == node_data.iloc[n+1,2]): # horizontal rightward
                    u = 0
                    v =  -1

            if (boundary_type == 1): # Left bank
                if (node_data.iloc[n,1] < node_data.iloc[n+1,1]) &
(node_data.iloc[n,2] > node_data.iloc[n+1,2]): #down right
                    u = abs(u)
                    v = abs(v)
                elif (node_data.iloc[n,1] > node_data.iloc[n+1,1]) &
(node_data.iloc[n,2] > node_data.iloc[n+1,2]): #down left
                    u = abs(u)
                    v = abs(v) * -1
                elif (node_data.iloc[n,1] < node_data.iloc[n+1,1]) &
(node_data.iloc[n,2] < node_data.iloc[n+1,2]): #up right
                    u = abs(u) * -1
                    v = abs(v)
                elif (node_data.iloc[n,1] > node_data.iloc[n+1,1]) &
(node_data.iloc[n,2] < node_data.iloc[n+1,2]): #up left
                    u = abs(u) * -1
                    v = abs(v) * -1
                elif (node_data.iloc[n,1] == node_data.iloc[n+1,1]) &
(node_data.iloc[n,2] > node_data.iloc[n+1,2]): #vertical down
                    u = 1
                    v = 0
                elif (node_data.iloc[n,1] == node_data.iloc[n+1,1]) &
(node_data.iloc[n,2] < node_data.iloc[n+1,2]): #vertical up
                    u = -1
                    v = 0
                elif (node_data.iloc[n,1] > node_data.iloc[n+1,1]) &
(node_data.iloc[n,2] == node_data.iloc[n+1,2]): #horizontal left
                    u = 0
                    v = -1
                elif (node_data.iloc[n,1] < node_data.iloc[n+1,1]) &
(node_data.iloc[n,2] == node_data.iloc[n+1,2]): #horizontal right
                    u = 0
                    v = 1
            xx.append(x) # midpoint coordinates
            yy.append(y)
            uu.append(u) # unit normal vector components
            vv.append(v)
        unit_vec=pd.DataFrame()
        unit_vec['x'] = (xx)
```

```
        unit_vec['y'] = (yy)
        unit_vec['u'] = uu
        unit_vec['v'] = vv

        return(unit_vec) # returns DataFrame of xx, yy, uu, vv

    # %% Run Unit Vectors Function for Left and Right Banks

    normals_rb = normals(boundary_type_r, sorted_rb_model_output)
    normals_lb = normals(boundary_type_l, sorted_lb_model_output)

    # %% Define Function for Calculation of Mass and Momentum

    def mass_momentum(boundary_types, node_data, unit_vectors):

        rho = 1000    # water density (kg/m3)
        i = len(unit_vectors.iloc[:,1])
        # Initialize lists to store results
        face_length = []
        face_area = []
        Q_lateral_ = []
        Q_lateral_per_unit_length_ = []
        Mass_transfer_flux_ = []
        Mass_flux_per_unit_length_ = []
        momentum_flux_per_area_ = []
        momentum_flux_ = []
        momentum_per_unit_length_ = []

        for n in range(0,i):
            # Now calculating parameters required for mass and momentum calculation
for mid-section of face (between nodes)
            uuu = unit_vectors.iloc[n,2]
            vvv = unit_vectors.iloc[n,3]
            length = sqrt(((node_data.iloc[n+1,1] - node_data.iloc[n,1])**2) +
((node_data.iloc[n+1,2] - node_data.iloc[n,2])**2)) # distance between nodes
            # Calculate average depth and velocity at midpoint between nodes
            depth = (node_data.iloc[n,3] + node_data.iloc[n+1,3]) / 2   # m
            vx = (node_data.iloc[n,4] + node_data.iloc[n+1,4]) / 2      # m/s
            vy = (node_data.iloc[n,5] + node_data.iloc[n+1,5]) / 2      # m/s
            area = length * depth                                       # m^2
            v_mag = sqrt((vx**2) + (vy**2))                             # m/s

            # Project velocity vector onto unit normal vector using dot product
            v_dot_n = vx * uuu + vy * vvv                               # m/s this
velocity is normal to the face boundary
            # Calculate volumetric flow rate across face
            Q_lateral = v_dot_n * area                                  # m^3/s
```

```
            Q_lateral_per_unit_length = Q_lateral / length              # m^3/s/m

            # Calculate mass transfer rate across face
            Mass_transfer_flux = rho * v_dot_n * area                   # kg/s or Nms
            Mass_flux_per_unit_length = Mass_transfer_flux / length     # kg/ms
            # Calculate momentum flux per unit area and momentum flux across face
            momentum_flux_per_area = rho * v_dot_n * abs(v_dot_n)        # N/m^2
            momentum_flux = rho * area * v_dot_n * abs(v_dot_n)          # N
            momentum_per_unit_length = momentum_flux / length;           # N/m

            # Store results
            face_length.append(length)
            face_area.append(area)
            Q_lateral_.append(Q_lateral)
            Q_lateral_per_unit_length_.append(Q_lateral_per_unit_length)
            Mass_transfer_flux_.append(Mass_transfer_flux)
            Mass_flux_per_unit_length_.append(Mass_flux_per_unit_length)
            momentum_flux_per_area_.append(momentum_flux_per_area)
            momentum_flux_.append(momentum_flux)
            momentum_per_unit_length_.append(momentum_per_unit_length)

        # Create ouptut DataFrame
        Mass_momentum = pd.DataFrame()
        Mass_momentum['x']=unit_vectors.iloc[:,0]
        Mass_momentum['y']=unit_vectors.iloc[:,1]
        Mass_momentum['face_length_m']=face_length
        Mass_momentum['face_area_m2']=face_area
        Mass_momentum['Q_lateral_m3_p_s']=Q_lateral_
        Mass_momentum['Q_lateral_per_unit_length_m2_p_s']=Q_lateral_per_unit_length_
        Mass_momentum['Mass_transfer_flux_kg_p_s']=Mass_transfer_flux_
        Mass_momentum['Mass_flux_per_unit_length_kg_p_ms']=Mass_flux_per_unit_length_
        Mass_momentum['momentum_flux_per_area_N_p_m2']=momentum_flux_per_area_
        Mass_momentum['momentum_flux_N']=momentum_flux_
        Mass_momentum['momentum_per_unit_length_Np_p_m']=momentum_per_unit_length_

        return(Mass_momentum) # Returns final dataframe

    # %% Run Mass and Momentum Functions for Left and Right Banks

    mass_momentum_rightBank =
mass_momentum(boundary_type_r,sorted_rb_model_output,normals_rb)
    mass_momentum_rightBank['bank'] = 'Right'

    mass_momentum_leftBank =
mass_momentum(boundary_type_l,sorted_lb_model_output,normals_lb)
    mass_momentum_leftBank['bank'] = 'Left'
```

```
    right_left_mass_momentum =
pd.concat([mass_momentum_rightBank,mass_momentum_leftBank])

    # Save results to .csv
    right_left_mass_momentum.to_csv(output_file_path)
    print('Results saved to:', output_file_path)

print('Done! :)')

# %%
```

7.3 Appendix C: Channel-Floodplain Flux

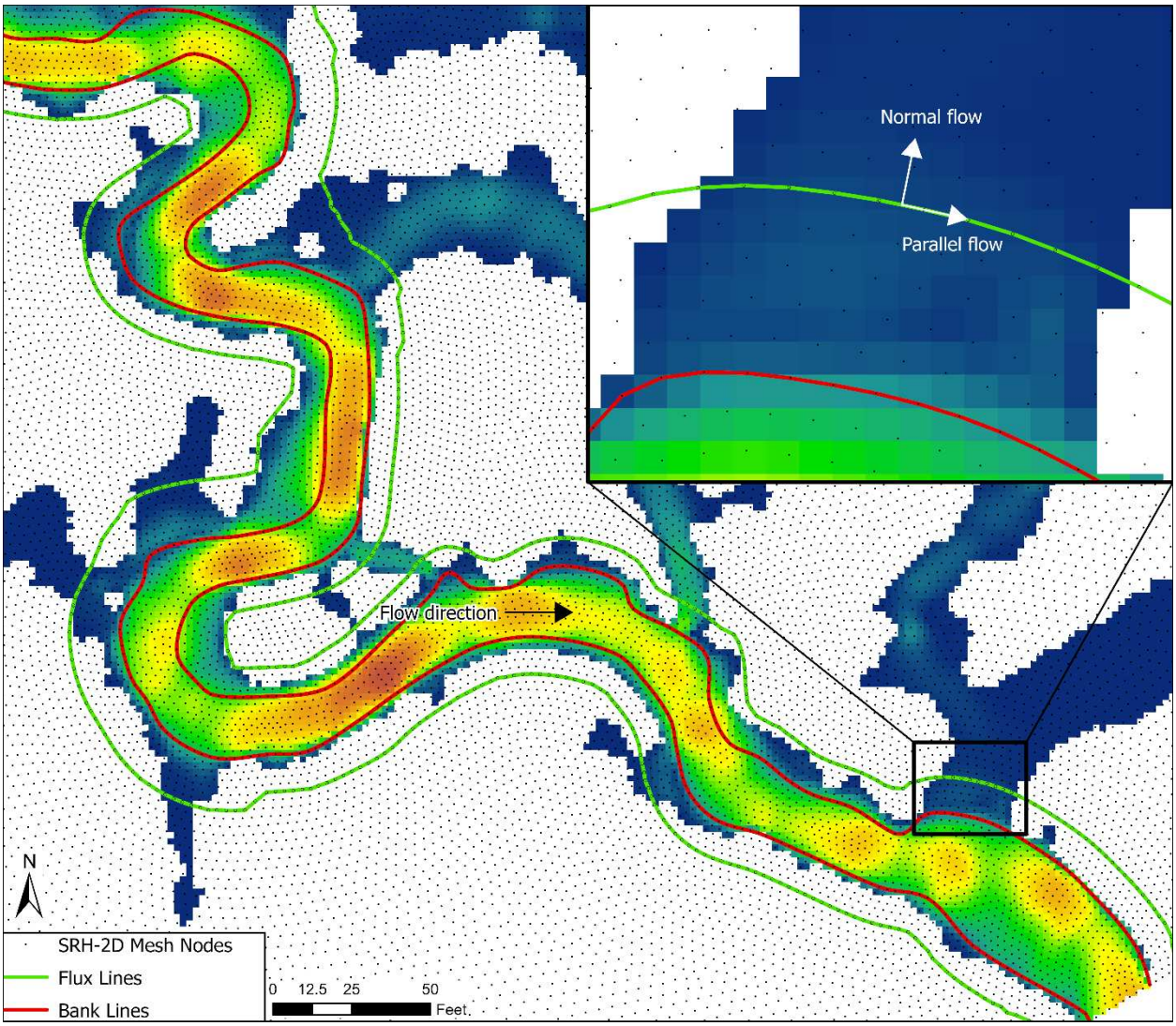

Figure C1. Example of how flux control surfaces were delineated relative the geomorphic bank lines and the 10-year velocity results at Lower Baker Creek.

7.4 Appendix D: Supplemental Model Results

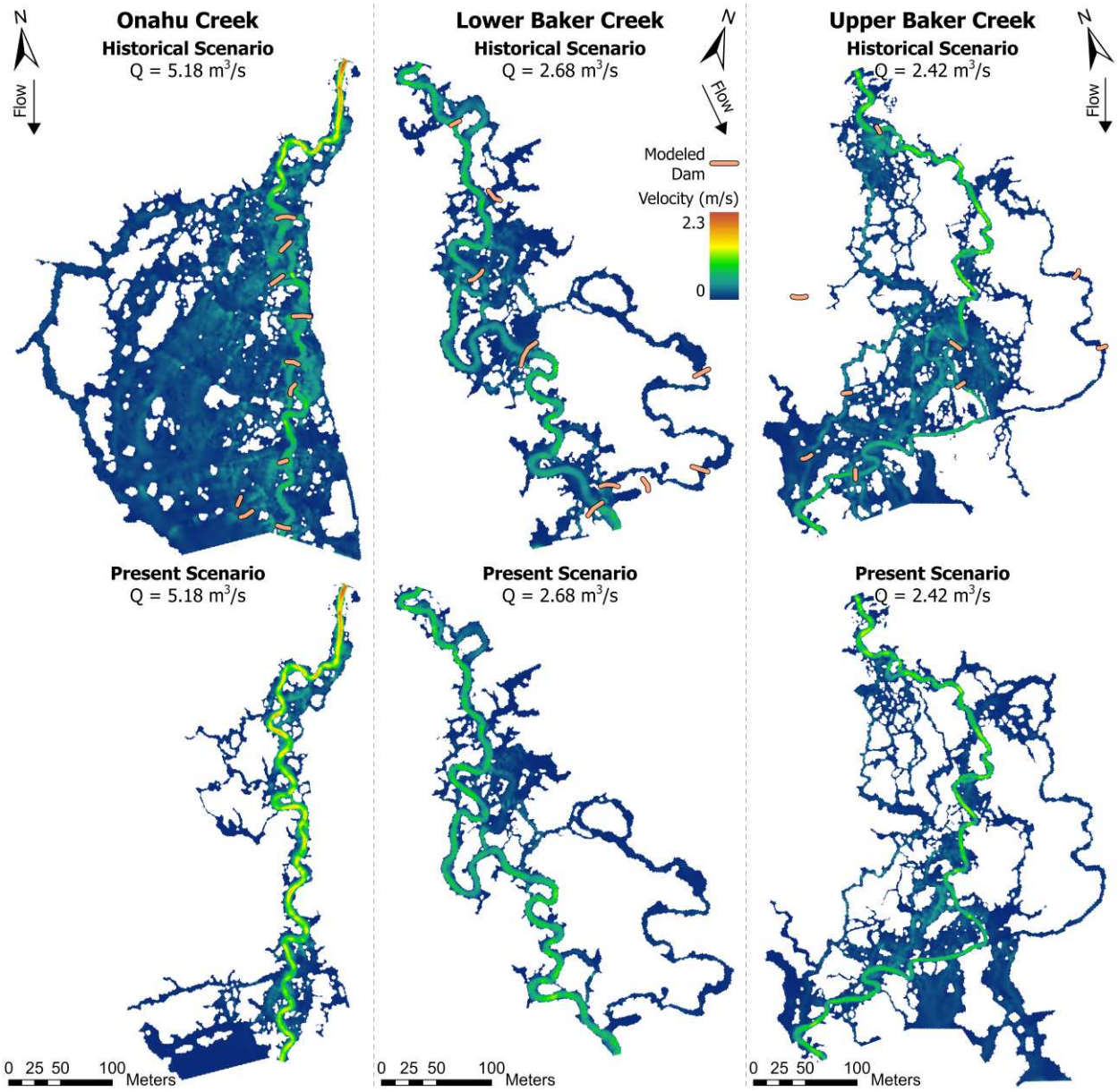

Figure D1. Steady-state velocity plots for the 5-year flood.

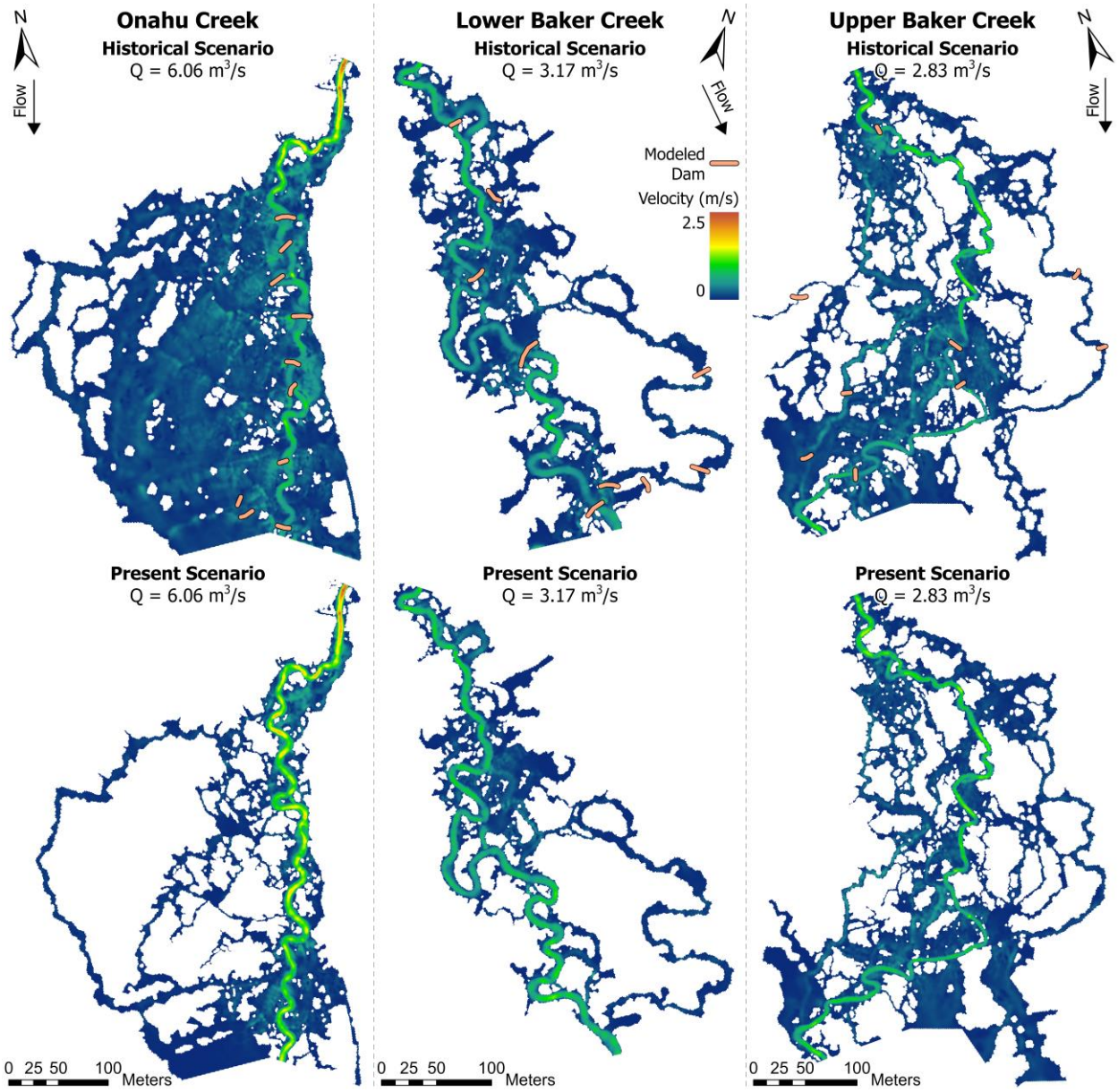

Figure D2. Steady-state velocity plots for the 10-year flood.

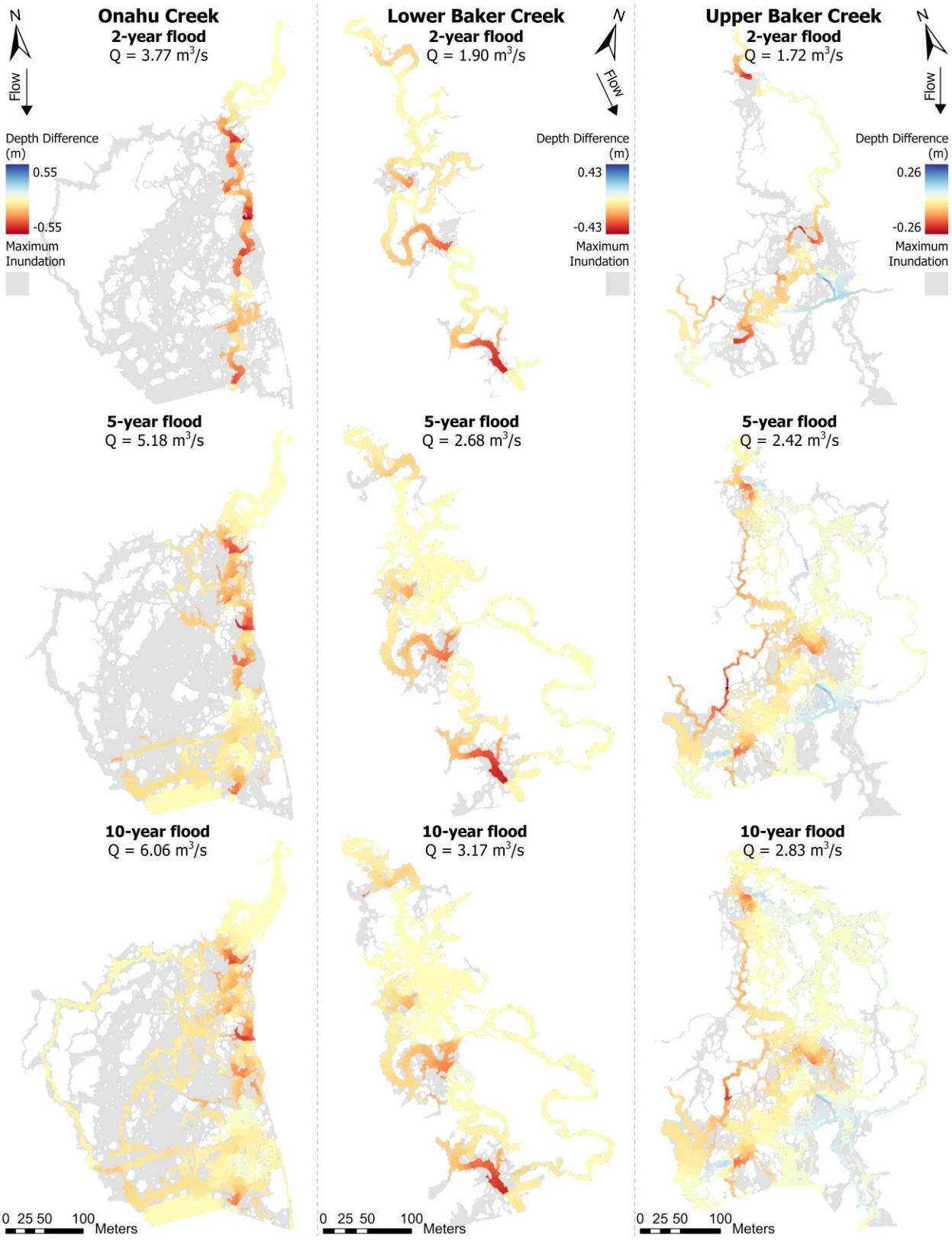

Figure D3. Depth difference plots (present minus historical conditions). Gray shading indicates areas that are inundated in only one scenario.

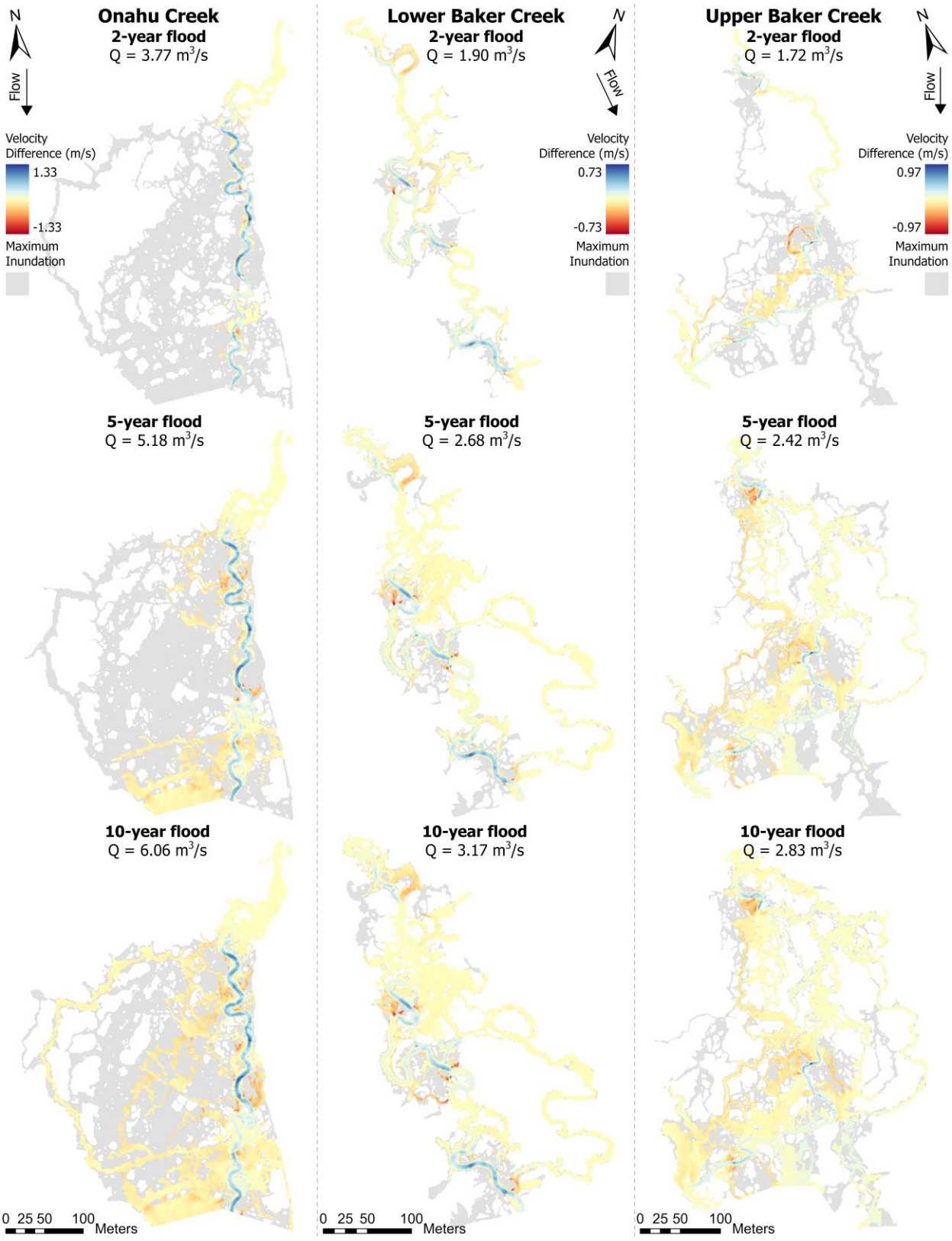

Figure D4. Velocity difference plots (present minus historical conditions). Gray shading indicates areas that are inundated in only one scenario.